Stratospheric Sensitivity to Perturbations in Ozone and Carbon Dioxide: Radiative and Dynamical Response

S. B. FELS, J. D. MAHLMAN, M. D. SCHWARZKOPF AND R. W. SINCLAIR

Geophysical Fluid Dynamics Laboratory/NOAA, Princeton University, Princeton, NJ 08540

(Manuscript received 17 December 1979, in final form 3 July 1980)

ABSTRACT

We have attempted to assess the stratospheric effects of two different perturbations: 1) a uniform 50% reduction in ozone; and 2) a uniform doubling of carbon dioxide. The primary studies employ an annual mean insolation version of the recently developed GFDL 40-level general circulation model (GCM). Supporting auxiliary calculations using purely radiative models are also presented. One of these, in which the thermal sensitivity is computed using the assumption that heating by dynamical processes is unaffected by changed composition, gives results which generally are in excellent agreement with those from the GCM. Exceptions to this occur in the ozone reduction experiment at the tropical tropopause and the tropical mesosphere.

The predicted response to the ozone reduction is largest at 50 km in the tropics, where the temperature decreases by 25 K; at the tropical tropopause, the decrease is 5 K. The carbon dioxide increase results in a 10 K decrease at 50 km, decreasing to zero at the tropopause. The temperature change in the CO_2 experiment is remarkably uniform in latitude.

1. Introduction

The possibility of an anthropogenically induced ozone reduction has been the subject of intense attention for the last decade. While many uncertainties remain, considerable progress has been made in elucidating the mechanisms which control the distribution of ozone, and therefore in our ability to assess the effects of various contaminants on the ozone layer. The results of these efforts are summarized in a series of assessment documents.[1,2,3,4,5,6]

In these reports, the problem of climatic response to ozone change received considerably less attention. This was, to a great extent, due to the lack of suitable models of the climate system. To date, the only systematic attempts to estimate possible climatic effects of ozone change have employed one-dimensional (1D) radiative-convective equilibrium models (e.g., Manabe and Wetherald, 1967; Luther *et al.*, 1977; Ramanathan, 1976; Ramanathan *et al.*, 1976; Reck, 1976; Ramanathan and Dickinson, 1979) or zonally symmetric models with highly simplified dynamics (Schoeberl and Strobel, 1978). Generally, the 1D models indicate substantial cooling of the upper stratosphere for large ozone reductions. Such models also indicate much smaller and more ambiguous temperature changes near the earth's surface.

In view of the possibility of large ozone reductions in the future, assessment of the associated climatic change is an important problem, which by its very nature must ultimately be addressed with interactive radiative-chemical-dynamical models of the atmosphere-ocean system. However, development of a climate model which is both reliable and comprehensive is still well in the future.

A closely related question is the possible climatic response to increasing atmospheric carbon dioxide amounts. Both problems require assessment of the climatic response to changes in an important radiatively active gas. In both cases, there remains substantial uncertainty as to what the long-term

[1] Grobecker, A. J., S. C. Coroniti and R. H. Cannon, 1974: Report of Findings: The effects of stratospheric pollution by aircraft. Final report, Climatic Impact Assessment Program, Department of Transportation DOT-TST-75-50 [NTIS AD/A-005 458/5SL].

[2] IMOS, 1975: Fluorocarbons and the environment. Report of Federal Task Force on Inadvertent Modification of the Stratosphere (IMOS). Council on Environmental Quality, Federal Council for Science and Technology [NTIS NSF-75-403].

[3] ICAS, 1975: The possible impact of fluorocarbons and halocarbons on ozone. Interdepartmental Committee for Atmospheric Sciences, Federal Council for Science and Technology, 109 pp. [NTIS PB-277 035/2SL].

[4] NAS, 1975: Environmental impact of stratospheric flight. National Academy of Sciences, Washington, DC [ISBN 0-309-02346-7].

[5] ——, 1976: Halocarbons: Effect on stratospheric ozone. National Academy of Sciences, Washington, DC [ISBN 0-309-02532-X].

[6] NASA, 1977: Chlorofluoromethane and the stratosphere. National Aeronautics and Space Administration, Scientific and Technical Information Office. NASA Ref. Publ. 1010, R. D. Hudson, Ed., 261 pp. [NTIS N77-31694/1GI].

perturbations in the trace constituent will be. Usually, however, assessment of carbon dioxide perturbations is thought to be simpler because its distribution in the atmosphere is nearly uniform, while ozone exhibits great variation in the vertical and the horizontal.

Although greatest attention has been paid to possible climatic change at and near the earth's surface, climate alteration in the stratosphere may prove to be a considerably larger effect (e.g., Manabe and Wetherald, 1967; Haigh and Pyle, 1979). Thus understanding of the stratospheric response to a perturbation in radiatively active trace constituents is important.

In addition, we believe that a reliable assessment of the stratospheric climatic response is fundamentally simpler to evaluate than that of the lower troposphere, since understanding the response of the lower troposphere probably depends on the capability to model properly the interactive atmosphere-ice-ocean systems. For modeling the stratospheric response, less caution is required, because, to an excellent approximation, the lower boundary ocean temperatures and "permanent" ice amounts can be prescribed at their present values. That is the approach taken in the work we present here. The relative simplicity of the stratospheric climatic response, along with the possibility that large changes in CO_2 or O_3 may occur in the near future, makes it interesting for its own sake.

In this paper the two separate problems analyzed are a uniform factor of 2 reduction in ozone amount and a uniform factor of 2 increase in carbon dioxide amount. The assumption of a uniform doubling of carbon dioxide amount is very reasonable because CO_2 is a well-mixed gas with relatively weak sources and sinks.

On the other hand, the question of determining the distribution of altered ozone amounts is enormously difficult. The present O_3 distribution is highly nonuniform and results from an interplay of chemical and transport processes. To the extent that the ozone amounts in the troposphere and lower stratosphere are determined solely by transport of O_3 downward from the mid-stratosphere photochemical equilibrium region, the assumption of a uniform percentage ozone reduction is a good one (Mahlman *et al.*, 1980). However, 1D models of O_3 reduction suggest a rather important column feedback effect (increased ozone production below the middle stratosphere due to a decreased ozone column above). This effect could become significant in the tropics.

The above considerations indicate that the stratospheric response to more realistic scenarios for ozone reduction is complex, since not only the response to a given change in O_3, but also the actual change in O_3 amount, must be determined. Consequently, we have adopted the more limited goal of understanding the stratospheric response in the hypothetical case of a uniform 50% reduction in O_3 from its present distribution.

For this purpose, we have chosen to examine the response of a series of models in which the seasonal cycle has been suppressed by use of annual average insolation. Although seasonal effects are of great importance in the middle stratosphere, the use of a seasonally varying insolation would have required longer model integrations than were possible. Moreover, results from an annual average insolation model provide a useful basis for interpreting the results of future studies in which the seasonal cycle is included.

In this study we use a new 40-level GFDL general circulation model (GCM) for the basic radiative-dynamical sensitivity experiments. Relevant aspects of this model are described in Section 2, while in Section 3 selected results of the control run simulation are discussed. To separate the purely radiative response from the more complex radiative-dynamical response, we present in Section 4 two supporting 1D radiative equilibrium model responses to the perturbations in O_3 and CO_2. These are based on the same radiative transfer algorithm used in the general circulation model, and allow us to evaluate the applicability of such simplified models to the type of stratospheric climate sensitivity questions posed here. Within the framework of such models, we also discuss the effects of including a highly parameterized model of temperature-dependent ozone chemistry.

In Section 5 we discuss the response of the dynamical model to the stratospheric perturbations, interpreting the results in light of the previously described radiative models.

2. Brief description of the general circulation model

The GCM used for this study is a modified version of the model presented by Holloway and Manabe (1971). The numerical schemes (see Kurihara and Holloway, 1967), convective adjustment, horizontal subgrid-scale diffusion, hydrology, realistic topography and surface boundary-layer processes are essentially the same as described in that paper.

There are a number of significant differences between this GCM and previous GFDL models. In the horizontal a latitude-longitude grid is utilized with Fourier filtering at higher latitudes to preserve uniformity of minimum longitudinal spatial scales (Holloway *et al.*, 1973). For this early experimentation, a coarse 9° latitude by 10° longitude grid is employed. More recent experiments are utilizing a higher horizontal resolution.

In the vertical the model contains 40 levels, with the top level at ~80 km. The vertical spacing slowly increases with altitude in such manner that

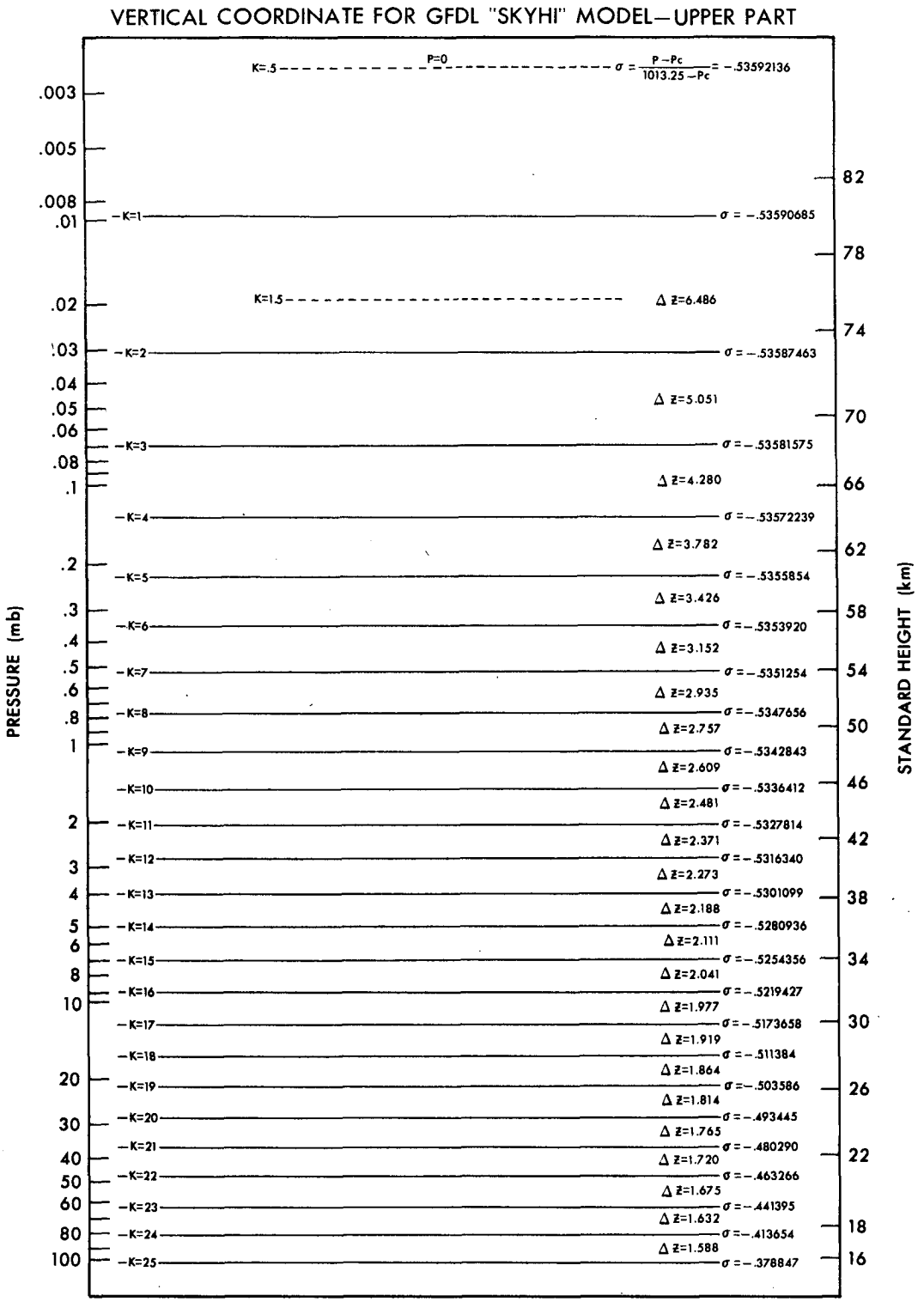

FIG. 2.1. Upper portion of the GCM vertical coordinate system, showing position of full and half levels. The standard height is based on a midlatitude standard atmosphere temperature sounding.

the ratio between any two adjacent level thicknesses is not too different from unity (see Figs. 2.1 and 2.2).

The vertical grid is a modified sigma (σ) system in which the lower tropospheric terrain-following surfaces slowly flatten with distance from the surface and become equivalent to isobaric surfaces above an arbitrary pressure p_c = 353.547851 mb (see Figs. 2.1

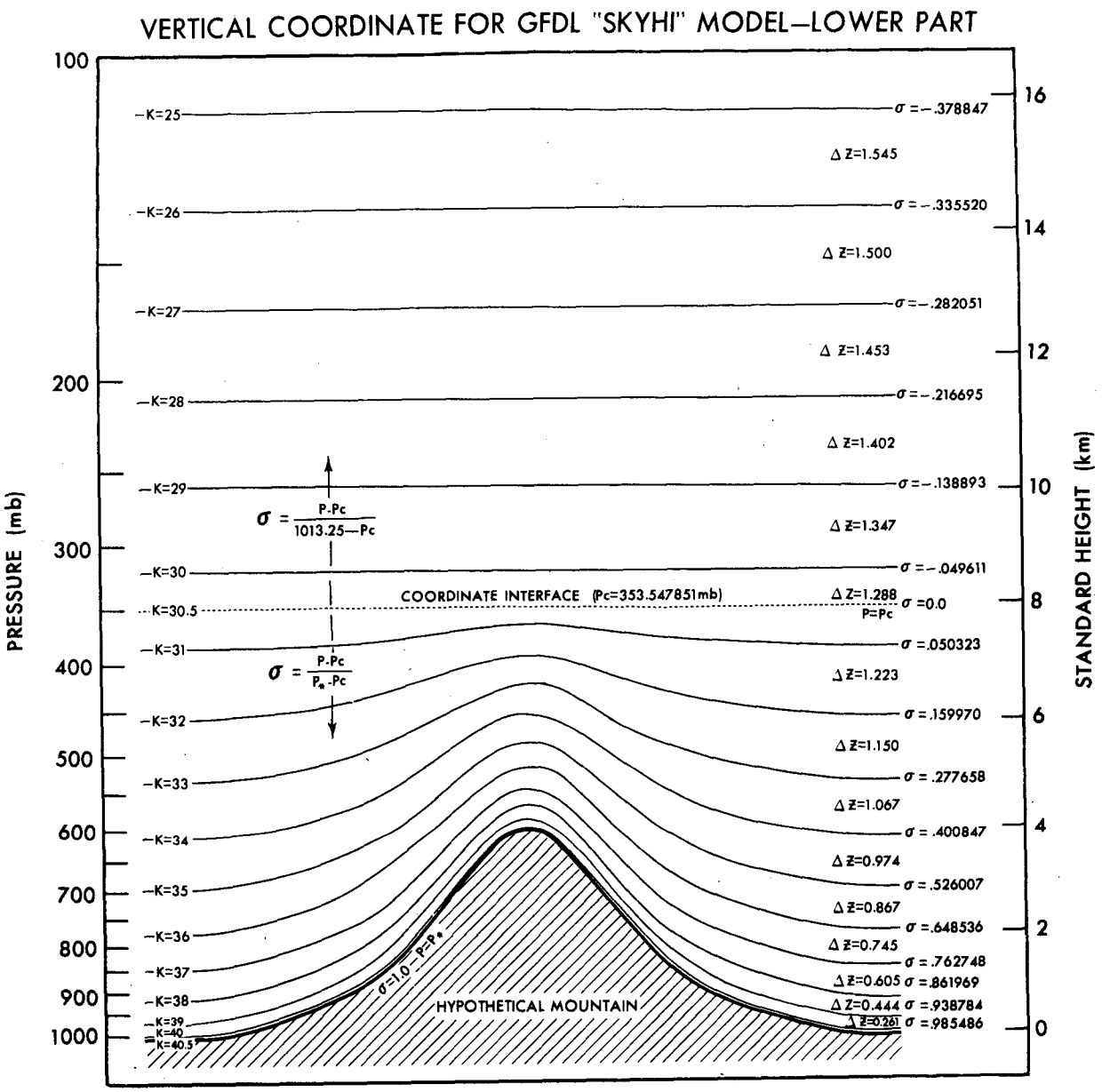

FIG. 2.2. Lower portion of the GCM vertical coordinate system, showing modified σ coordinate. Above 353.547851 mb, the vertical structure is unaffected by topography.

and 2.2). The values of σ are defined as

$$\sigma = \frac{p - p_c}{p_* - p_c}, \qquad p > p_c, \tag{2.1}$$

$$\sigma = \frac{p - p_c}{1013.25 - p_c}, \qquad p < p_c, \tag{2.2}$$

where p_* is the surface pressure, and all pressures are expressed in millibars. Figs. 2.1 and 2.2 show that the approximate vertical resolution is 1 km in the middle troposphere, 1.5 km in the lower stratosphere, 2 km in the middle stratosphere and 3 km near the stratopause. This coordinate was developed at GFDL by S. Manabe and J. L. Holloway, Jr., using ideas of Sangster (1960). The coordinate offers a number of important advantages in a model which contains a number of levels above the troposphere. The analysis of the model atmosphere above 350 mb can be done exactly in isobaric coordinates thereby avoiding the error introduced in transforming from σ to p coordinates (Mahlman and Moxim, 1976). The model can execute with greater speed because the required transformations from σ to p for pressure gradient and horizontal diffusion terms can be avoided.

Also, such an approach avoids the undesirable oscillations induced in stratospheres of σ coordinate models whenever strong winds occur near large slopes in the σ surfaces.

At the lower and upper boundaries the vertical σ velocity ($d\sigma/dt$) is set to zero. At the ground this constrains the flow to follow the topography. At the upper boundary ($p = 0$) this corresponds to the so-called "lid condition", which under some circumstances can lead to spurious reflections of upward propagating waves. The impact of this boundary is "softened" somewhat through incorporation of a parameterized diffusion of eddy quantities through the top model level into a hypothetical thermosphere.

We have run various tests of model sensitivity to this and other more elaborate upper boundary conditions. In each case we found that the model stratosphere is almost completely insensitive to the choice of upper boundary condition applied above the top (~80 km) level. On the other hand, the meteorological structure at the top model level is significantly influenced by the choice of upper boundary condition. By 60 km, however, the sensitivity is minimal.

The vertical subgrid-scale transfer is evaluated through use of a diffusion coefficient which includes a functional dependence on the Richardson number and a parameterization of the effect of vertical grid size. The scheme is designed to be applicable from the boundary layer to the mesopause. Because of the scheme's minimal influence on the results presented here, details will be presented in a later publication.

Infrared radiation is calculated through use of the methods of Fels and Schwarzkopf (1975, 1980).[7] The shortwave heating employs the parameterization proposed by Lacis and Hansen (1974) with heating due to O_2 absorption included.[8] To conserve computer time, radiation is calculated only once every 12 model hours, with the calculated rates applied uniformly over the 12 h period. As noted earlier, the radiative transfer algorithms used in the GCM are identical to those employed in the radiative equilibrium calculations.

Self-determined prognostic quantities in the model are wind, temperature, water vapor, ground temperature, soil moisture, snow cover and surface pressure. Cloudiness, pack ice and the ocean surface temperature are prescribed. This prescription, of course, acts to constrain the troposphere to remain nearer its present climatic structure than would be the case if these constraints were removed.

Carbon dioxide is fixed at a constant 330 parts per million by volume (ppmv) in the control and halved ozone experiments, and 660 ppmv in the perturbed CO_2 experiment.

Ozone is prescribed between the ground and 34 km. Between 34 and 80 km (model levels 1–15), the region where local photochemical equilibrium is nearly achieved, the ozone mixing ratio is allowed to "float" from the prescribed value as the local photochemical equilibrium responds to local temperature fluctuations. This change in local photochemical equilibrium arises from the temperature dependence of some of the key kinetic reactions in the ozone continuity equation. This process is crudely parameterized by a method outlined in Appendix A. Inclusion of these processes in the calculations presented here is important because the mechanism leads to an acceleration of the rate that a temperature perturbation relaxes to radiative-photochemical equilibrium and to significant changes in the stratospheric sensitivity to increased CO_2.

The prescribed O_3 field is presented in Fig. 2.3. At 30 km and below it is taken from Hering and Borden.[9] Their time-averaged seasonal data are subjectively analyzed over the North American network, taking into account level-by-level consistency. From these charts the zonal average is inferred by allowing for the apparent longitudinal asymmetries and the known meteorological structure in that region of the atmosphere. Above 30 km the available data deteriorate markedly in quality, especially in the mesosphere. In this region the basic prescribed ozone amounts are set to be those values which give a reasonable vertical temperature profile in low latitudes. The meridional structure is guided by the Nimbus 4 BUV data of Heath.[10] Above 30 km, this base ozone prescription of Fig. 2.3 can be considered in part to be an adjustable parameter of the model which "covers" for the other errors in the upper stratosphere radiative balance calculations.

3. Selected GCM results

The GCM was initially integrated from a resting, isothermal state for 500 days with annually and diurnally averaged insolation. Throughout the extra-

[7] The 9.6 μm O_3 lines are treated as Lorentz lines. A companion experiment employing the method of Fels (1979) to treat these lines shows minimal differences from the present work.

[8] Data to calculate this heating were supplied by H. Levy II (1979, private communication), and are based on cross sections and fluxes derived from Ackerman (1971).

[9] Hering, W. S., and T. R. Borden, 1967: Ozonesonde Observations over North America, Vol. 4. *Environ. Res. Pap.*, No. 279, AFCRL-64-30 (IV), Air Force Cambridge Research Laboratories, 365 pp. [NTIS AD-666 436].

[10] Heath, D. F., 1974: Recent advances in satellite observations of solar variability and global atmospheric ozone. NASA Goddard Space Flight Center, X-912-74-190, Greenbelt, MD, 39 pp. [NTIS N74-30286/OGI].

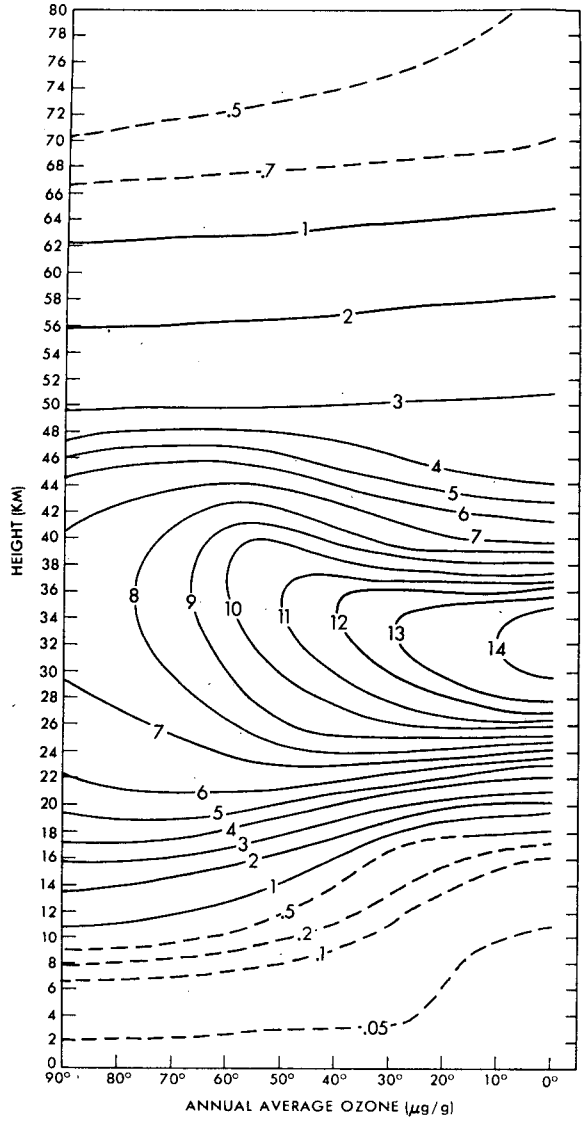

FIG. 2.3. Prescribed ozone mass mixing ratio for control runs ($\mu g\ g^{-1}$). The field is an annual average, and is assumed to be symmetrical about the equator.

tropical atmosphere, statistical equilibrium existed in the temperature and wind fields. At this point, the control and the two perturbed versions were integrated for an additional 220 days.

All analyses presented in this work are 120-day averages of data sampled daily from the final 120 days of each integration. The vertical coordinate structure used in this GCM eliminates any errors due to vertical interpolation above 350 mb. Detailed analysis indicates that time sampling is not a significant source of error.

Although it is not the purpose of this paper to discuss details of the simulation results, a discussion of the basic-state GCM structure is of some importance. This is because the credibility of the sensitivity analyses is dependent on the reliability of the simulated physical processes leading to the control statistical equilibrium state.

There is some question as to what constitutes a "good" stratospheric simulation in a model using annual mean insolation. In view of the well-known monsoonal character of the stratosphere, an average of the seasonal structures could be quite different from the structure arising in response to an annual mean radiation. As mentioned previously, however, we choose to analyze the annual mean case for reasons of economy and ease of interpretation.

The zonal mean temperature simulated by the model and the corresponding "observed" temperatures are given in Fig. 3.1. The observed state between 30 and 80 km is taken from CIRA (1965). Below 30 km, we have used an annual average based on Newell *et al.* (1972). There are many uncertainties in the observations, especially in high latitudes where data are sparse. It is not clear, for example, how seriously one should regard the reversed gradient poleward of 60° near the stratopause. While the overall agreement of model and observation is not bad, the observed reversed gradient in the upper mesosphere is not successfully simulated. Results from recent experiments using higher horizontal resolution suggest that this may be due in part to the relatively large horizontal viscosity used in the low-resolution model.

In the lower stratosphere, the GCM successfully simulates a reversed meridional temperature gradient. (For contrast see the radiative-convective equilibrium temperature field in Fig. 4.3.) The equatorial tropopause is somewhat too cold in the model. Consequently, the reversed meridional temperature gradient in the lower stratosphere is slightly too strong. The lower tropospheric temperatures agree closely with observations, as might be expected in view of the prescribed ocean surface temperatures.

An especially interesting feature of Fig. 3.1b is the high-latitude stratospheric temperature field. Up to the middle stratosphere, at least, the "cold bias" of previous GFDL GCM's (see Manabe and Hunt, 1968; Manabe and Mahlman, 1976) is apparently no longer present. A series of companion experiments suggests that it is the increased vertical resolution of the present model that reduces this bias. At higher altitudes, there is evidence that a cold bias remains in the polar regions.

The simulated zonal winds are presented in a later section in Fig. 5.3a and are essentially in geostrophic balance with the temperature field of Fig. 3.1b. The tropospheric zonal winds contain some significant defects. The zonal wind maxima corresponding to the subtropical jet streams are somewhat too weak and are located too close to the equator. The tropical upper tropospheric westerlies are too

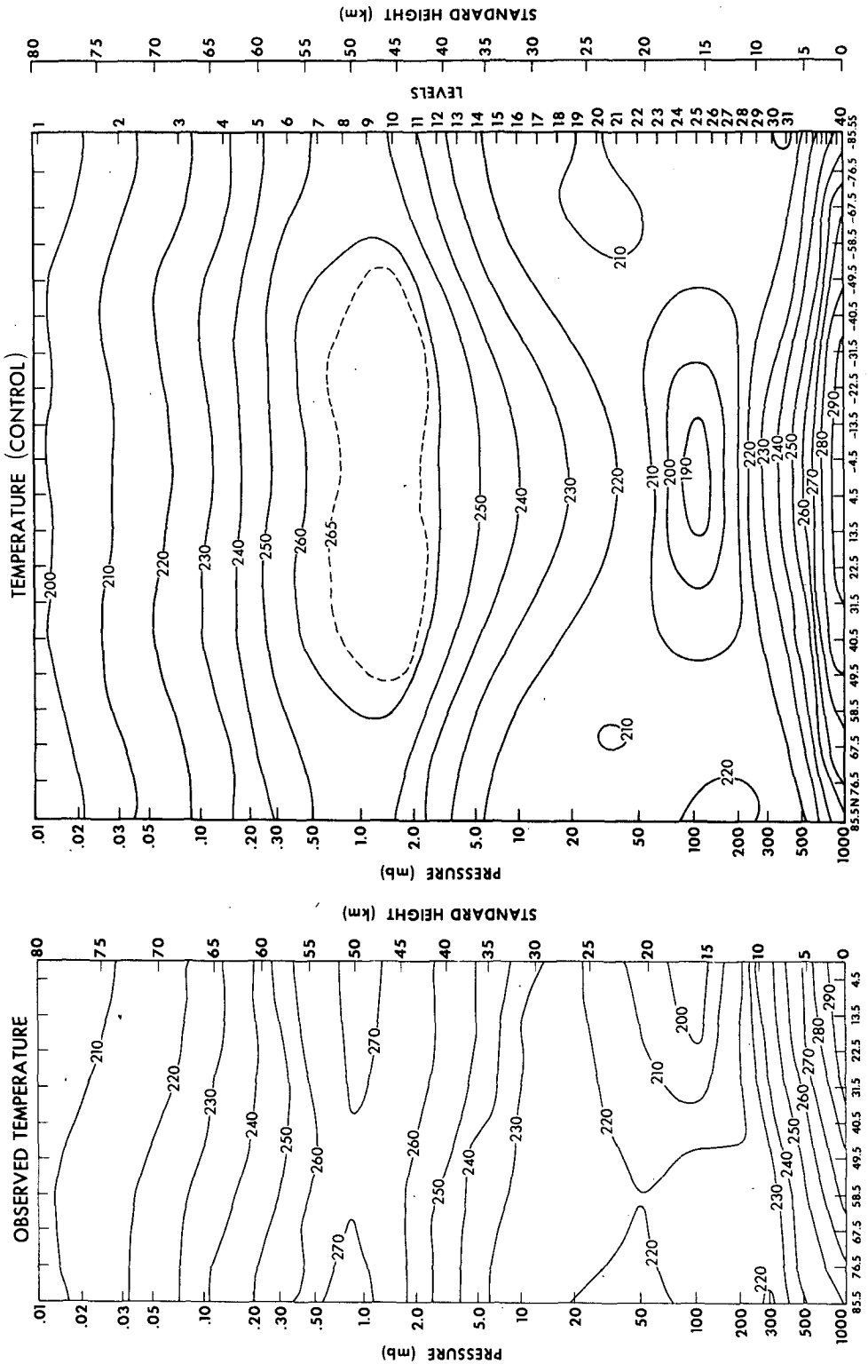

FIG. 3.1. Observed annual-average zonal mean temperature (a) for the Northern Hemisphere; and simulated annual-average zonal mean temperature (b) from the GCM control run.

strong, while the midlatitude surface westerlies are nearly missing. These are all defects which appear to be related to the coarse horizontal resolution.

A notable result of the simulation of zonal winds shown in Fig. 5.3a is the presence of equatorial westerlies near 40 km, with easterlies above in the mesosphere. The model analysis shows that these westerlies are produced and maintained by a vertical convergence of eddy momentum flux.[11] The large-scale eddies responsible for this flux appear to be equatorial Kelvin waves, primarily of zonal wavenumber 1. A more detailed analysis of the eddy fluxes is in progress.

Careful examination of the tropical mesospheric wind field reveals the existence of trends of long time scale.[11] Between days 660 and 720, for example, the longitudinal mean of the zonal wind component, $\bar{U}$, changes from about -10 to 0 m s^{-1} at 68 km. In light of this, some caution must be exercised in interpreting sensitivity results in this region of the model atmosphere.

4. Radiative model results

a. General considerations

In considering problems which involve perturbations of radiatively active atmospheric constituents, it is convenient to think of two extreme possible responses of the actual atmosphere. These have been called "radiative" and "dynamical" adjustment in slightly different contexts (Fels and Kaplan, 1975; Ramanathan and Dickinson, 1979). Consider a statistically equilibrated atmosphere in which the sum of shortwave heating (which has little temperature dependence) and longwave cooling (which is strongly temperature dependent) is balanced by dynamical heating or cooling ($Q_{\rm dyn}$):

$$J_{\rm sw} + Q_{\rm lw}(T) + Q_{\rm dyn} = 0. \qquad (4.1a)$$

Suppose now that we change $J_{\rm sw}$ (by changing the ozone mixing ratio, for example). In the new equilibrium, we have

$$J'_{\rm sw} + Q'_{\rm lw}(T') + Q'_{\rm dyn} = 0, \qquad (4.1b)$$

or for small changes

$$\delta J_{\rm sw} + \frac{\delta Q_{\rm lw}}{\delta T}\,\delta T + \delta Q_{\rm dyn} = 0. \qquad (4.2)$$

We shall say that the adjustment is purely radiative if $\delta Q_{\rm dyn} = 0$, and purely dynamical if $\delta T = 0$. In practice, of course, the response of the atmosphere will involve changes in both δT and $\delta Q_{\rm dyn}$.

There are several circumstances under which changes in the dynamical heating rates might be expected. The simplest of these occurs when the local thermal structure is convectively controlled, in which case the rate of vertical heat transfer due to convection will change in response to changes in $J_{\rm sw}$, while the temperature remains fixed. Of considerably more theoretical interest are responses which involve changes in the large-scale dynamical heating, due either 1) to changes in the meridional structure of $J_{\rm sw}$ or 2) to changes in the eddy structure in the atmosphere.

In the case of a large alteration in the horizontal structure of $J_{\rm sw}$, it is reasonable to expect changes in the mean meridional circulation, and therefore changes in $Q_{\rm dyn}$. The situation is complicated, however, by the constraints placed on the system by rotation. A simple model (presented in Appendix C) suggests that the response to a symmetric change in $\partial J_{\rm sw}/\partial y$ will be primarily dynamical in the tropics and radiative in the extratropics.

Dynamical adjustment may also come about through changes in eddy fields. It has been suggested by several authors (e.g., Dickinson, 1974; Schoeberl and Geller, 1977) that there exists in the stratosphere a complex nonlinear coupling of dynamical and radiative processes, which can be described as follows. The dynamical heating is due largely to meridional heat fluxes induced by upward propagating planetary waves generated in the troposphere. The structure of these waves may depend importantly on the structure of the mean zonal wind field, which in turn, is determined by the mean thermal field through geostrophy. The thermal wind field is therefore in part established by the dynamical heating which it helps determine. In such a situation, one would expect that changes in composition might lead to important changes in $Q_{\rm dyn}$.

To the extent that the actual adjustment is purely radiative, however, it is predictable without making use of elaborate dynamical models. We shall therefore begin our discussion of stratospheric composition perturbations by considering the response of two models in which changes in dynamical heating are either neglected altogether, or parameterized extremely crudely. Since, throughout much of the middle atmosphere, the primary balance is between shortwave heating by O_3 and longwave cooling by CO_2, there is reason to hope that such models may give a good first-order picture of the true response. Moreover, by comparing these results with those from the GCM experiments, we will be able to discover whether the latter show any important dynamical adjustment, and so decide whether the hypothetical tight coupling of dynamics and radiation discussed above does in fact exist.

In discussing these radiative models, it is useful to have available a simple scheme to aid in inter-

[11] Mahlman, J. D., and R. W. Sinclair, 1980: Recent results from the GFDL troposphere-stratosphere-mesosphere general circulation model. *Proceedings of the IAMAP-ICMUA Session on Modeling of the Stratosphere and Mesosphere*. IUGG XVII General Assembly, Canberra, Australia, December 1979 (to be published).

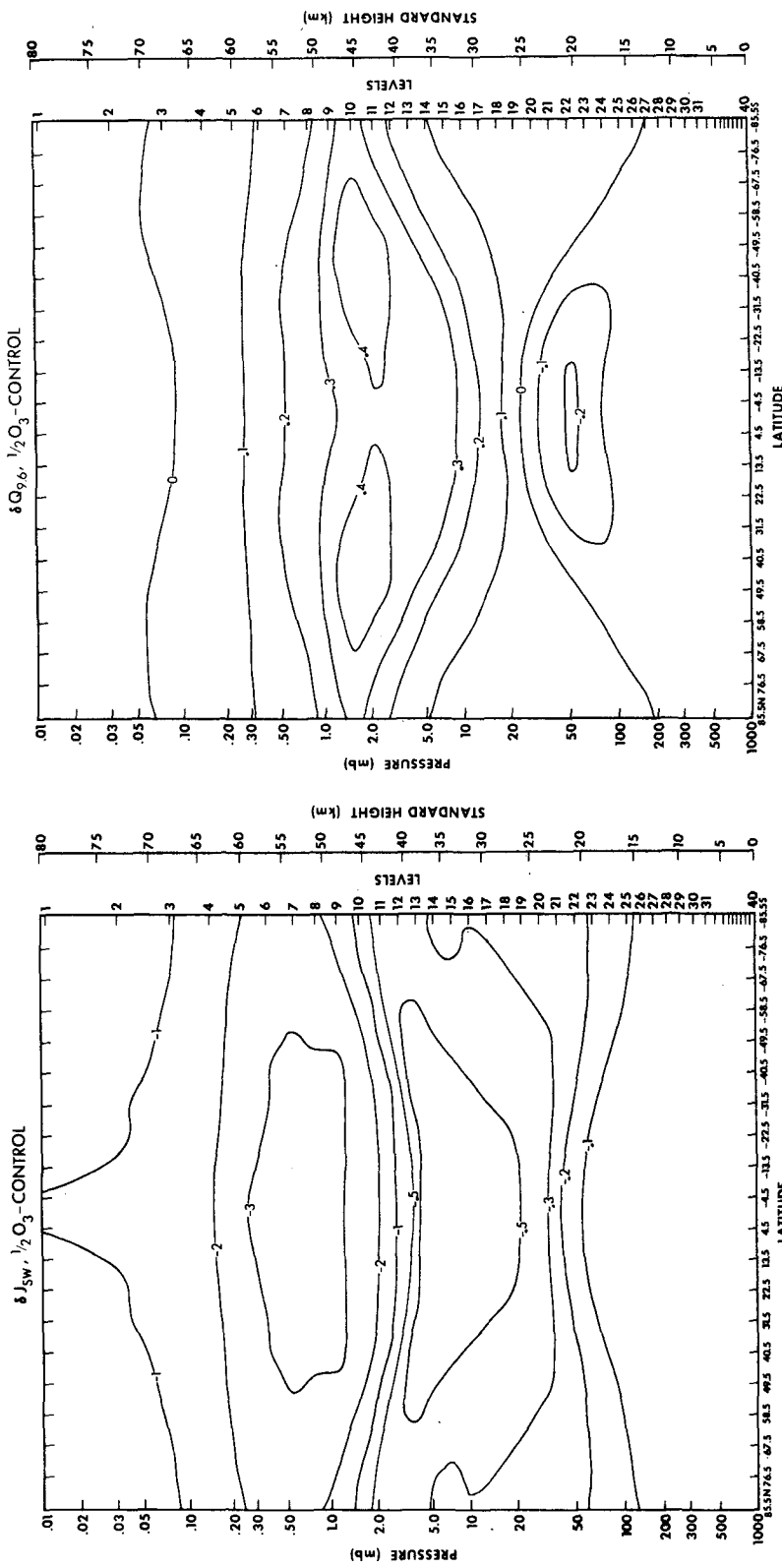

FIG. 4.1. Radiative drives (K day^{-1}) for the ozone reduction experiments: (a) δJ_{sw}, the change in shortwave heating due to a 50% ozone reduction; and (b) $\delta Q_{9.6}$, the change in 9.6 μm O_3 band heating rate due to a 50% ozone reduction, with the temperatures in all cases held fixed at the control values.

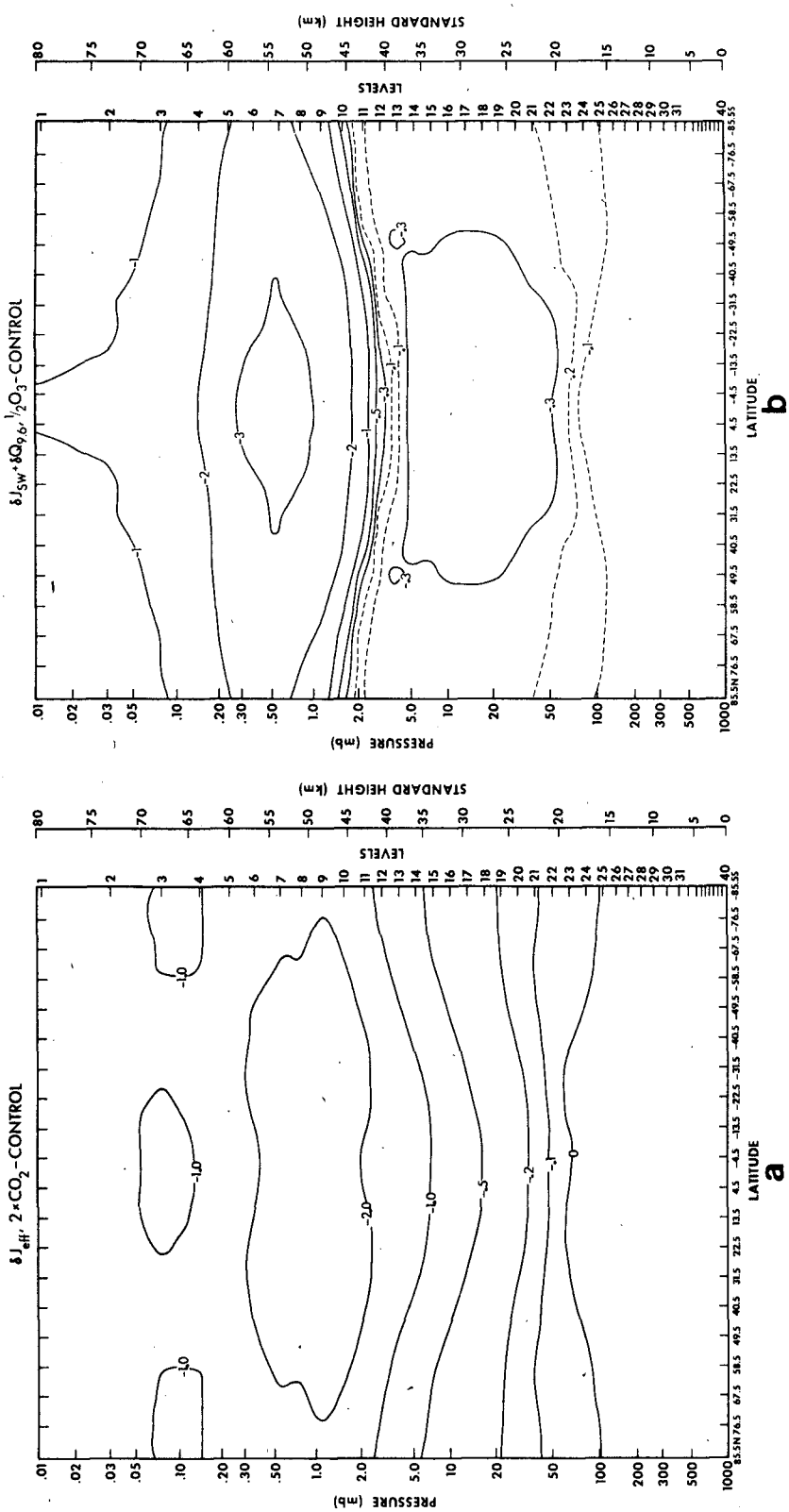

FIG. 4.2. Total radiative drives (K day^{-1}) for the $\frac{1}{2}O_3$ and $2 \times CO_2$ experiments: (a) $(\delta J)_{\text{eff}}$, the change in 15 μm CO_2 band heating rate due to a doubling of CO_2, the temperatures being held fixed at the control values; and (b) $\delta J_{sw} + .\delta Q_{9.6}$, the total drive for the ozone reduction experiment.

preting the results, one which not only helps explain the response actually found, but can also be used to suggest what sort of results might be obtained in other, different experiments. In Appendix B, we discuss in some depth the general considerations which determine the radiative response to a change in the ozone or carbon dioxide amounts. For the reader who is not concerned with that level of detail, we summarize the results briefly here:

1) The temperature change $\delta T(p)$ due to changed composition is an approximately local function of the form

$$\delta T(p) = cT^2 \exp(960/T) \times \text{"Drive"},$$

where c is approximately independent of temperature.

2) In the case of altered ozone amounts, "Drive" consists of two pieces: (i) δJ_{sw}, the change in shortwave heating, and (ii) $\delta Q_{9.6}$, the change in 9.6 μm IR heating/cooling. These are shown in Fig. 4.1 and their sum in Fig. 4.2b.

3) In the altered CO_2 case, "Drive" is the change in longwave cooling rates due to changed CO_2 mixing ratio at fixed temperature; this is referred to as $(\delta J)_{eff}$ and is shown in Fig. 4.2a.

4) The factor of $T^2 \exp(960/T)$ means that for a given "Drive," the response is largest at low temperature; this will be referred to as the "temperature effect", and suggests the importance of the correct choice of unperturbed thermal structure in sensitivity experiments.

b. The latitudinal radiative-convective equilibrium (RCE) model

If we neglect all horizontal transports, both by the atmosphere and the ocean, and further assume that the annual average thermal structure is the steady-state response to the annual average insolation, we are led to consider a situation in which each latitude is in radiative-convective equilibrium. As is conventional, we shall assume that the critical convective lapse rate is 6.5 K km^{-1}. A fixed relative humidity profile, the same for all latitudes, is assumed below 20 mb, while above the water mixing ratio is fixed at 3.2 ppmv. Fig. 4.3 shows the thermal structure which results from such a model, in which a series of ten independent radiative-convective equilibria are computed, each latitude having its own ozone distribution (Fig. 2.3) and appropriate annual mean insolation and cloud structure. The surface temperature is not prescribed, but determined self-consistently by the requirement of energy balance. Comparison with the observed annual thermal structure (Fig. 3.1a) shows that large differences exist in the troposphere and lower stratosphere, with the tropics too warm and the poles too cold. It is especially worth noting that this model does not produce the reversed meridional thermal gradient in the lower stratosphere. This is a distortion which has important consequences, as we shall see shortly.

When using this model in sensitivity experiments, we fix the surface temperature at its unperturbed value so that the response is purely radiative above the convective zone and purely dynamical below. This is in contrast to a different sort of model, to be discussed later, which can only respond radiatively. For this reason, the RCE model is of some interest, in spite of its shortcomings.

1) RESPONSE TO OZONE REDUCTION

Above 35 km, the thermal sensitivity (Fig. 4.4a) depends largely on the local response to $\delta J_{sw} + \delta Q_{9.6}$ mentioned previously (Fig. 4.2b). In particular, the strong meridional gradients of δT near 50 km reflect those of δJ_{sw} in this region. These temperature gradients are reduced somewhat by the temperature $[T^2 \exp(960/T)]$ effect. For example, at 55 km, the ratio $(\delta J_{sw} + \delta Q_{9.6})^{equator}/(\delta J_{sw} + \delta Q_{9.6})^{polar} \approx 1.5$, while $\delta T^{equator}/\delta T^{polar} \approx 1.2$. The colder polar temperature (246 K vs 268 K at the equator), which thus accentuates its temperature response to its "Drive," accounts for the rest of this difference.

Below 35 km, however, there occurs an interesting reversal in the meridional gradient of δT, with the larger sensitivity in the polar regions. This is evidently not a simple response to the local structure of $\delta J_{sw} + \delta Q_{9.6}$; at 30 km, for example, this driving term is actually twice as large at the equator as at the pole. The reversal is the result of two causes: nonlocality of response and the local temperature effect.

Nonlocality simply means that δT at one height responds to $\delta J_{sw} + \delta Q_{9.6}$ at others; the fact that it is important in this region suggests that the reversal at 30 km may really be a reflection of what is going on below. Indeed, at 16 km the driving term is larger at the poles than at the equator so that, for this reason alone, we expect a larger polar δT.

Of greater importance, however, is the fact that in the tropics the convective region penetrates to above 15 km, while in the polar regions it only penetrates to ~8 km. The tropical temperatures near 15 km are therefore very tightly constrained, while those in the polar regions are free to change. This can be very clearly seen in Fig. 4.4a, where the dashed lines indicate the top of the convective zone. The $\delta T = 0$ K isopleth nearly coincides with these, and the $\delta T = -2$, -4 and -6 K isopleths are roughly parallel. The nonlocality of the response tends to communicate the temperature variation at 15 km to the middle stratosphere, thus explaining to some degree the structure of δT near 30 km.

The second reason for the enhanced polar δT is

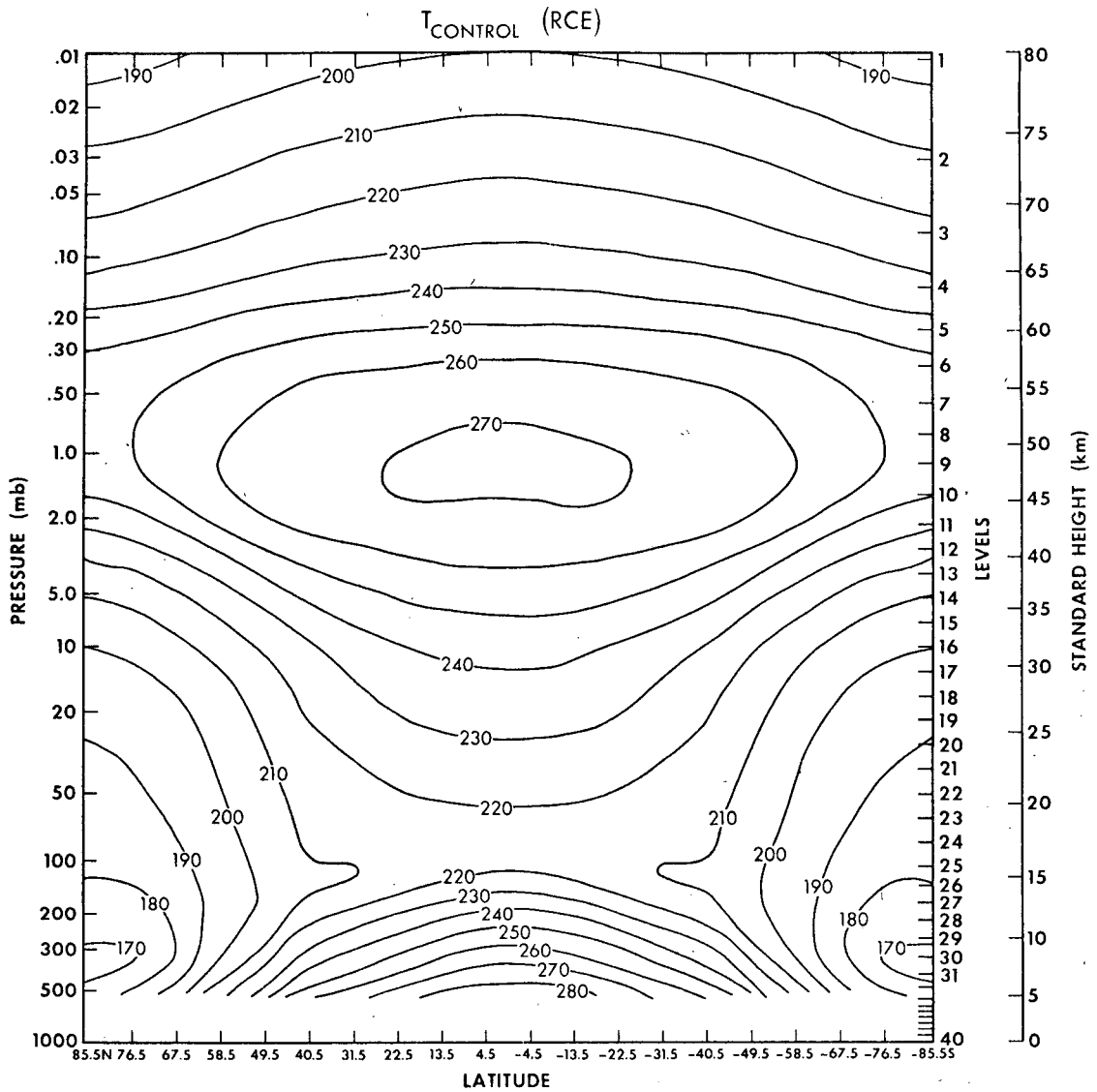

FIG. 4.3. Equilibrium stratospheric and mesospheric temperature for the radiative-convective equilibrium (RCE) control experiment.

the temperature effect. Throughout the region below 35 km, the RCE model has polar temperatures from 30 to 45 K colder than those at the equator. This means that even for the same drive, the polar sensitivities will be larger by ~1.6 than those at the equator. Since the real atmosphere is warmer at the poles than at the equator at these heights, the validity of the sensitivity results, in the lower stratosphere, at least, is very dubious. In fact, as we shall see shortly, use of a more realistic base state, and relaxation of the constraint of a ≤ 6.5 K km^{-1} lapse rate gives completely different results.

2) Response to carbon dioxide increase

Compared to the ozone reduction results, δT for the 2 × CO_2 case is smaller and more uniform meridionally, as Fig. 4.5a shows. We have already mentioned that the thermal response depends largely on $(\delta J)_{\text{eff}}$ (cf. Fig. 4.2a). Above 28 km, the sensitivity is greatest in the tropics, reflecting the equatorial maximum in $(\delta J)_{\text{eff}}$. The meridional gradient of δT in the middle and upper stratosphere is actually smaller than one would expect from an examination of $(\delta J)_{\text{eff}}$. There are two reasons for this. The temperature effect enhances the sensitivity of the colder polar regions relative to that in the tropics (e.g., by a factor of 1.2 at 50 km). Of equal importance is the effect of the parameterized ozone photochemistry in the model, which acts to increase the ozone heating preferentially in the tropics. This will be discussed more fully in Section 4d.

Although at 50 km $(\delta J)_{\text{eff}}$, the primary drive for the 2 × CO_2 experiment, is smaller than $\delta J_{\text{sw}} + \delta Q_{9.6}$

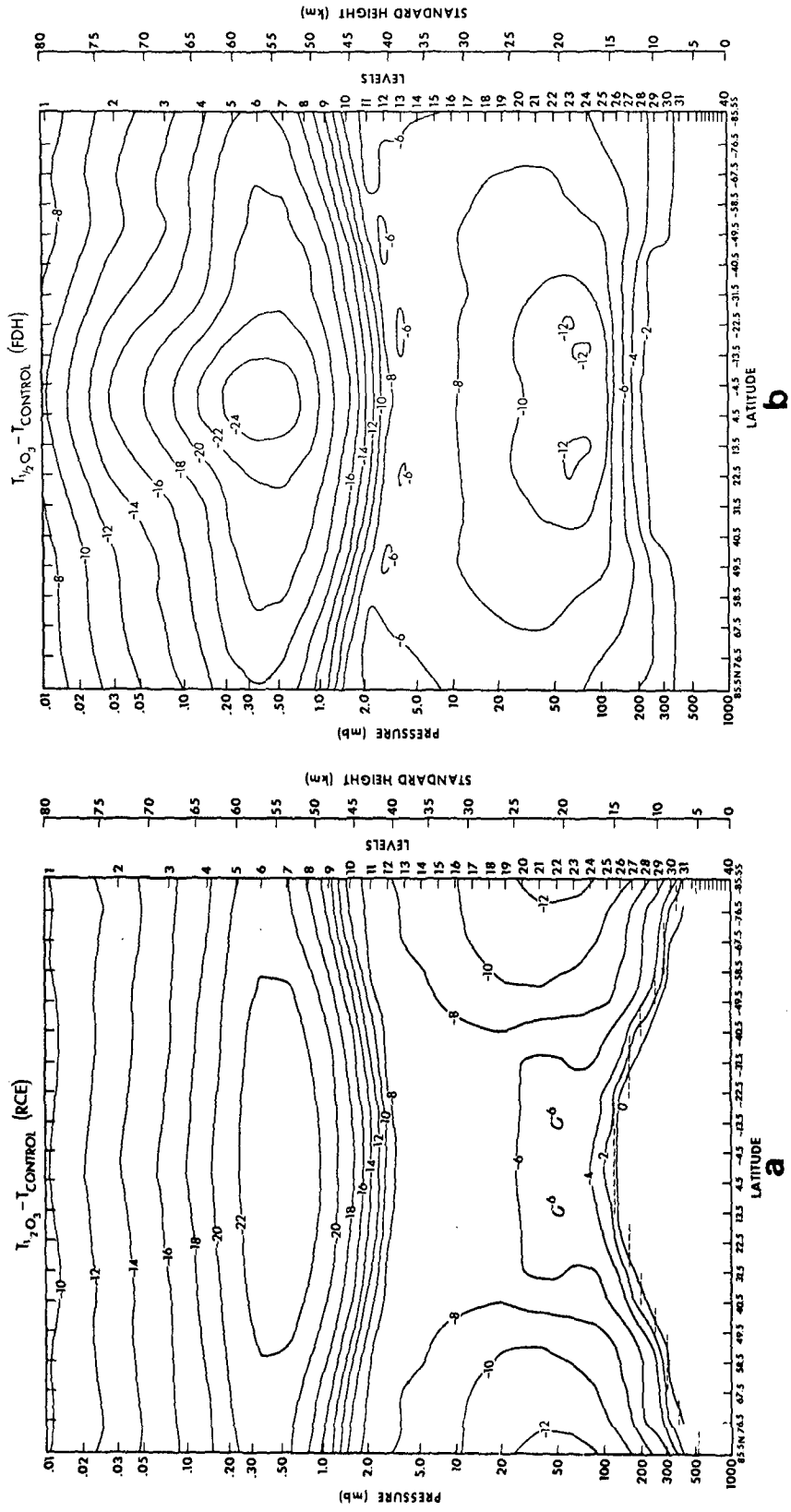

FIG. 4.4. Temperature change due to 50% ozone reduction ($\delta T = T_{1/2O_3} - T_{\text{control}}$), as simulated by (a) the RCE model and (b) the FDH model.

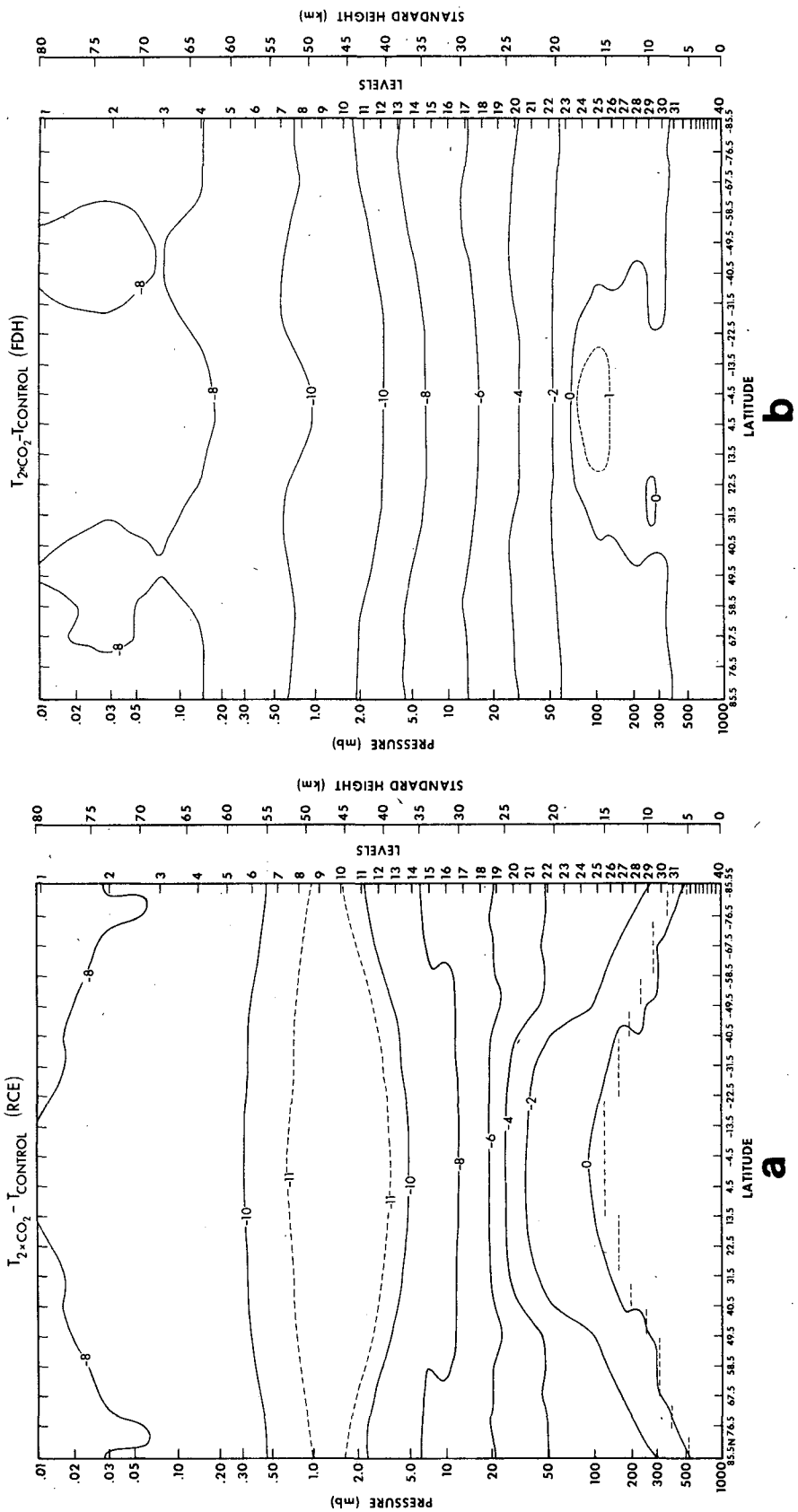

FIG. 4.5. Temperature change due to doubled CO_2 ($\delta T = T_{2\times CO_2} - T_{control}$), as simulated by (a) the RCE model and (b) the FDH model.

(the drive for the $\frac{1}{2}O_3$ experiment) by a factor of only 0.69, the temperature change in the $2 \times CO_2$ case is -10 K as opposed to -24 K in the $\frac{1}{2}O_3$ case. This smaller sensitivity is due partly to the ozone chemistry effect mentioned above, and partly to the smaller response of a $2 \times CO_2$ atmosphere than a standard atmosphere to a given drive, as discussed in Appendix B.

In the lower stratosphere, below 28 km, there is again a reversed gradient in δT, with the largest values near the poles. Referring to Fig. 4.2a, it will be seen that this is *not* a local effect, for between 28 and 22 km, $(\delta J)_{\text{eff}}$ is largest in the tropics. Just as in the ozone reduction case, the reversed gradient is due to both the temperature effect and reduced sensitivity due to a deeper convective region in the tropics.

c. *The latitudinal radiative model with fixed dynamical heating (FDH)*

The strong dependence of the calculated temperature sensitivity on the assumed basic state, which we have discussed earlier, suggests that a better radiative model would be one which forces the unperturbed state to be more realistic. A simple method of doing this is to take the desired base state and calculate the total radiative heating $J_{\text{sw}} + Q_{\text{lw}}$ at each point. By assumption this is the negative of the dynamical heating required to maintain this state. Given a knowledge of this dynamical heating, it is now possible to do sensitivity studies in which the dynamical heating is assumed to remain constant, i.e., in which the adjustment is purely radiative in the sense discussed earlier.

This is very simply implemented in practice. The same radiative code used for the previous experiment is modified by 1) turning off the convective adjustment routine; 2) fixing the surface temperature at the desired value; and 3) including in the temperature tendency equation a term equal to the dynamical heating at the point in question. (This will, of course, depend on latitude and height, in general.)

While it might seem best to use the observed thermal structure for the unperturbed state, it is actually more appropriate for the purposes of this study to use the unperturbed state generated by the control run of the GCM. It happens that the GCM gives a fairly realistic representation of the annual mean structure of the atmosphere, so that we need not worry too much about distortions of actual thermal sensitivity introduced by use of the "wrong" unperturbed state. A much more important reason for using the GCM generated state is that we will, by comparison with the GCM sensitivity, be able to assess how good the assumption of radiative adjustment is in practice.

The GCM temperature field for present values of O_3 and CO_2 has already been discussed (Fig. 3.1b). The total radiative heating rates generated from it are shown in Fig. 5.2a. We shall not comment on the temperature structure in this section. It is worth noticing, however, that in most of the middle atmosphere, dynamical heating is a small fraction of either the shortwave or longwave radiative components; a notable exception is at the tropical tropopause, a point to which we will return later.[12]

To perform sensitivity studies with the FDH model, we simply make the appropriate perturbation in the radiation routine and solve, for each of the 10 latitudes used before, the radiative equilibrium

$$J'_{\text{sw}} + Q'_{\text{lw}}(T') + Q_{\text{dyn}} = 0 \qquad (4.3)$$

for the perturbed temperature T'.

1) Response to ozone reduction

Above 30 km the results of the present (FDH) model (Fig. 4.4b) are similar to those found with the RCE model (Fig. 4.4a), although the meridional gradient of δT is now somewhat larger in the tropics. Between 30 and 16 km, however, there is a radical difference between the two models; the sensitivity is now largest in the tropics. At 20 km, for example, δT is -11 K at the equator, and only -7 K near the poles, whereas the corresponding RCE sensitivities are -12 K at the pole and -6 K at the equator.

There are two factors which largely account for this difference. The first is the relaxation of the 6.5 K km^{-1} lapse rate constraint, which allows the tropical temperature at 15 km to respond to a given forcing as freely as do those at 15 km in the polar regions. The second is the temperature effect. In the FDH model, the polar temperature at 20 km is 215 K, while in the RCE model it is 185 K. On the basis of the temperature effect alone, therefore, δT in the FDH model should be only 65% of what it is in the RCE model at the pole. The situation in the tropics is somewhat more complex. We have already pointed out that above 18 km, $\delta J_{\text{sw}} + \delta Q_{9.6}$ is larger in the tropics than at the poles (cf. Fig. 4.2b); therefore, in the absence of convective constraint, δT should be largest near the equator. Furthermore, below 22 km, the temperatures near the equator are much lower than those at high latitudes. For example, the equatorial temperature at 20 km is 178 K, the polar temperature 215 K. The temperature effect becomes especially important between 15 and 18 km, where $\delta J_{\text{sw}} + \delta Q_{9.6}$ is actually smaller in the tropics than

[12] This result may be peculiar to the annual average atmosphere; at the Southern Hemisphere polar night stratopause, for example, dynamical cooling rates on the order of 8 K day^{-1} exist (Hartmann, 1976).

TABLE 4.1. Difference in shortwave heating (δJ_{sw}) and in 9.6 μm O_3 heating ($\delta Q_{9.6}$)(K day^{-1}) due to 50% ozone reduction, with the temperature held fixed at the GCM control value. Values are given for the polar and equatorial latitudes in the 14–34 km region. The total radiative drive, $\delta J_{sw} + \delta Q_{9.6}$ is also included.

Level	Standard height (km)	85.5°N			4.5°N		
		δJ_{sw}	$\delta Q_{9.6}$	$\delta J_{sw} + \delta Q_{9.6}$	δJ_{sw}	$\delta Q_{9.6}$	$\delta J_{sw} + \delta Q_{9.6}$
15	34.0	−0.25	0.07	−0.18	−0.71	0.33	−0.38
16	31.9	−0.29	0.08	−0.21	−0.63	0.23	−0.40
17	29.9	−0.28	0.06	−0.22	−0.63	0.18	−0.45
18	28.0	−0.27	0.05	−0.22	−0.58	0.10	−0.48
19	26.2	−0.26	0.04	−0.22	−0.49	0.01	−0.48
20	24.3	−0.25	0.03	−0.22	−0.35	−0.08	−0.43
21	22.6	−0.23	0.03	−0.20	−0.22	−0.17	−0.39
22	20.9	−0.22	0.03	−0.19	−0.12	−0.20	−0.32
23	19.2	−0.19	0.03	−0.16	−0.06	−0.16	−0.22
24	17.5	−0.15	0.02	−0.13	−0.02	−0.07	−0.09
25	16.0	−0.11	0.01	−0.10	−0.01	−0.03	−0.04
26	14.4	−0.08	0.01	−0.07	−0.00	−0.02	−0.02

near the poles; in spite of this δT is still larger in the tropics. This is partly due to the action of nonlocal forcing from above, as well as to the temperature effect.

The important role played by the 9.6 μm ozone band in determining the sensitivity is perhaps surprising, and is illustrated in Table 4.1. We show there the terms δJ_{sw} and $\delta Q_{9.6}$ for latitudes 85.5 and 4.5°N. It is interesting that in the tropics $\delta Q_{9.6}$ is larger in magnitude than δJ_{sw} below 22 km. Without this term, therefore, the sensitivity of the lower tropical stratosphere (above 17 km) would actually be less in the tropics than at high latitudes.

A possible deficiency in the FDH model is the lack of constraint on the lapse rate. In fact, in the tropics between 14 and 15 km, the perturbed lapse rate slightly exceeds -9.8 K km^{-1}, the dry adiabatic lapse rate. (The control lapse rate cannot, since it is derived from a GCM with convective adjustment.) To assess the significance of this effect, we have performed a companion experiment in which the lapse rate of the FDH model is also constrained to be less than the dry adiabatic. The results show surprisingly little change in the FDH sensitivities; at 13 km the sensitivity is reduced by ~1 K, while at 16 km by 0.6 K; above this there is virtually no change.

The FDH ozone-reduction experiment is very similar to one performed by Ramanathan and Dickinson (1979), but our results differ substantially from those of their Fig. 6. While the general structure is similar in the two calculations, they find significantly smaller changes in temperature due to a 30% O_3 reduction than would be estimated from our results. We do not fully understand the reason for these differences. Ramanathan and Dickinson hold the tropospheric temperature fixed, which, as we have already seen, reduces the size of δT in the lower stratosphere. There are doubtless other effects such as differences in the radiative transfer models, cloud parameterization and unperturbed ozone amounts which contribute to the discrepancy.

2) RESPONSE TO CARBON DIOXIDE INCREASE

In broad outline, the thermal sensitivity (Fig. 4.5b) of the FDH model is similar to that of the RCE model discussed previously. Above 25 km, the discrepancies are quite minor and of little importance. Below this, however, several interesting differences do appear: there is a region of slight warming near the tropical tropopause in the FDH model, which is clearly a local response to the slightly positive $(\delta J)_{eff}$ in that region. This occurs below the convective boundary of the RCE model, and therefore has no effect there. It will also be noted that the $\delta T = -2$ K line is very flat in the FDH model, while in the RCE case it has a noticeable downward tilt near the poles. The low sensitivity in the polar regions between 10 and 17 km is largely due to the very small values of $(\delta J)_{eff}$ there and to the relatively warm polar temperatures.

d. Effects of parameterization of ozone mixing ratio

All of the previously discussed models include an algorithm designed to simulate crudely the effects of temperature-dependent ozone destruction reactions. Through this device, the model ozone mixing ratios above 34 km can vary from their initially prescribed values. The amount of variation depends on the deviation of the local temperature from an assumed radiative equilibrium temperature. This parameterization, which is described in Appendix A, was contrived so that the control experiment ozone mixing ratios differ little from those

shown in Fig. 2.3, and the $\frac{1}{2}O_3$ mixing ratios are very close to half those of Fig. 2.3. By arranging the experiments in this manner, what we have previously referred to as $\frac{1}{2}O_3$ experiments are just that. The effects of the parameterized chemistry in the $\frac{1}{2}O_3$ cases are therefore negligible, and require no further discussion.

Increase of CO_2, on the other hand, can be expected to result in changed O_3 levels, and the experiments we have performed reflect this. To determine the effect of the ozone parameterization, we have undertaken an FDH $2 \times CO_2$ experiment in which the O_3 is fixed at its value in the control experiment. Substantial differences between this and the previous experiment are observed. Table 4.2 shows the altered temperature sensitivity and the change in ozone mixing ratio for the equatorial and polar latitudes. The principal results are not surprising: the parameterized chemistry acts to increase the O_3 and therefore to decrease the temperature sensitivity. This decrease is significant; at the stratopause it is close to 30%.

In the no-chemistry case, δT at 50 km is 1 K greater at the equator than at the poles, in qualitative agreement with the forcing provided by $(\delta J)_{\text{eff}}$. When the parameterization is introduced, the ozone mixing ratio is changed. This results in an additional forcing from the change in shortwave heating. According to Table 4.2, the fractional increase in O_3 is relatively uniform ($\sim$10%) at all latitudes and heights. The forcing resulting from this change may be inferred from Fig. 4.1a; for a uniform fractional increase, δJ_{sw} is largest at the equator in the 35–80 km region. The meridional gradient in this δJ_{sw} therefore acts to counter the gradient in $(\delta J)_{\text{eff}}$ to produce the rather flat profile of δT shown in Fig. 4.5b and Table 4.2.

Our results are qualitatively similar to those of Luther *et al.* (1977), Boughner (1978), Groves *et al.* (1978) and Haigh and Pyle (1979). At the stratopause level, the change in O_3 as well as the temperature sensitivity is roughly similar to that reported by the previous work. The total column density of ozone increases by 1.5% in equatorial latitudes but by slightly <1% in polar regions. It should be pointed out that the present scheme leaves unchanged the ozone mixing ratios below 35 km, unlike some previous work.

The preceding results indicate that incorporation of a scheme to parameterize the change in ozone mixing ratios due to photochemical interaction produces significant changes in the resulting thermal structure of the model. Since results from the GCM and FDH models closely resemble each other, this finding lends justification and importance to the inclusion of this process in general circulation models.

TABLE 4.2. Fractional change in ozone ($\delta O_3/O_3$) resulting from use of the ozone parameterization in the FDH $2 \times CO_2$ experiment. Temperature sensitivity (K) in the standard (with chemistry) and no-chemistry cases, at equatorial and polar latitudes.

Level	Standard height (km)	$\frac{\delta(O_3)}{O_3}$	δT^*	δT^{**}
		Equatorial (4.5°N) point		
3	68.3	0.092	−7.4	−10.0
4	64.0	0.090	−7.6	−10.6
5	60.2	0.094	−8.3	−11.6
6	56.8	0.098	−8.8	−12.3
7	53.7	0.104	−9.4	−12.8
8	50.7	0.108	−9.8	−13.0
9	48.0	0.112	−10.1	−13.0
10	45.4	0.114	−10.3	−12.5
11	42.9	0.117	−10.5	−11.9
12	40.5	0.113	−10.1	−10.9
13	38.2	0.103	−9.2	−9.9
14	36.1	0.096	−8.5	−9.1
		Polar (85.5°N) point		
3	68.3	0.101	−7.8	−9.6
4	64.0	0.097	−7.9	−10.1
5	60.2	0.101	−8.6	−11.1
6	56.8	0.105	−9.2	−11.7
7	53.7	0.111	−9.8	−12.1
8	50.7	0.115	−10.1	−12.0
9	48.0	0.121	−10.6	−12.0
10	45.4	0.122	−10.6	−11.3
11	42.9	0.112	−9.6	−10.1
12	40.5	0.106	−8.8	−9.3
13	38.2	0.100	−8.1	−8.5
14	36.1	0.097	−7.6	−8.0

* With ozone parameterization.
** Without ozone parameterization.

5. General circulation model results

a. Response to ozone reduction

1) CHANGES IN TEMPERATURE STRUCTURE

For the most part, the temperature sensitivity of the GCM (Fig. 5.1b) is rather similar to that of the fixed dynamical heating model (Fig. 5.1a) discussed earlier—indeed, near the stratopause it is difficult to find any significant difference between the two. However, there are two regions where the dynamical model differs importantly from the radiative model, implying that the dynamical heating/cooling has not remained constant. The first of these is between 55 and 75 km in the tropics, where the horizontal gradient of δT is actually reversed in the GCM relative to the FDH model. This is a reflection of the substantially reduced dynamical cooling in this region, as Fig. 5.2 illustrates. This change in the dynamical cooling seems to be mani-

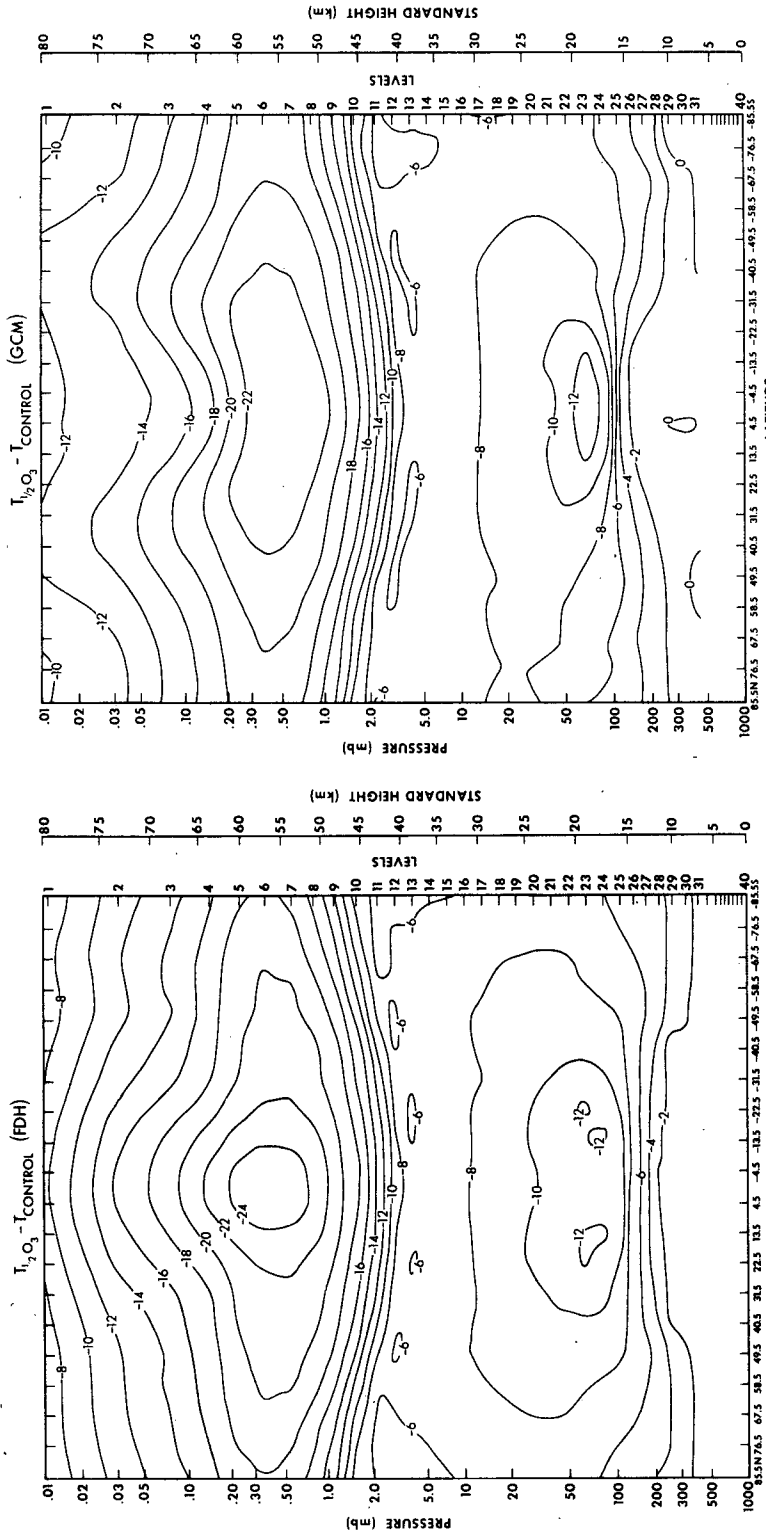

FIG. 5.1. Temperature change due to 50% ozone reduction as simulated by (a) the FDH model and (b) the GCM. The GCM results in this and subsequent figures are based on a 120-day average.

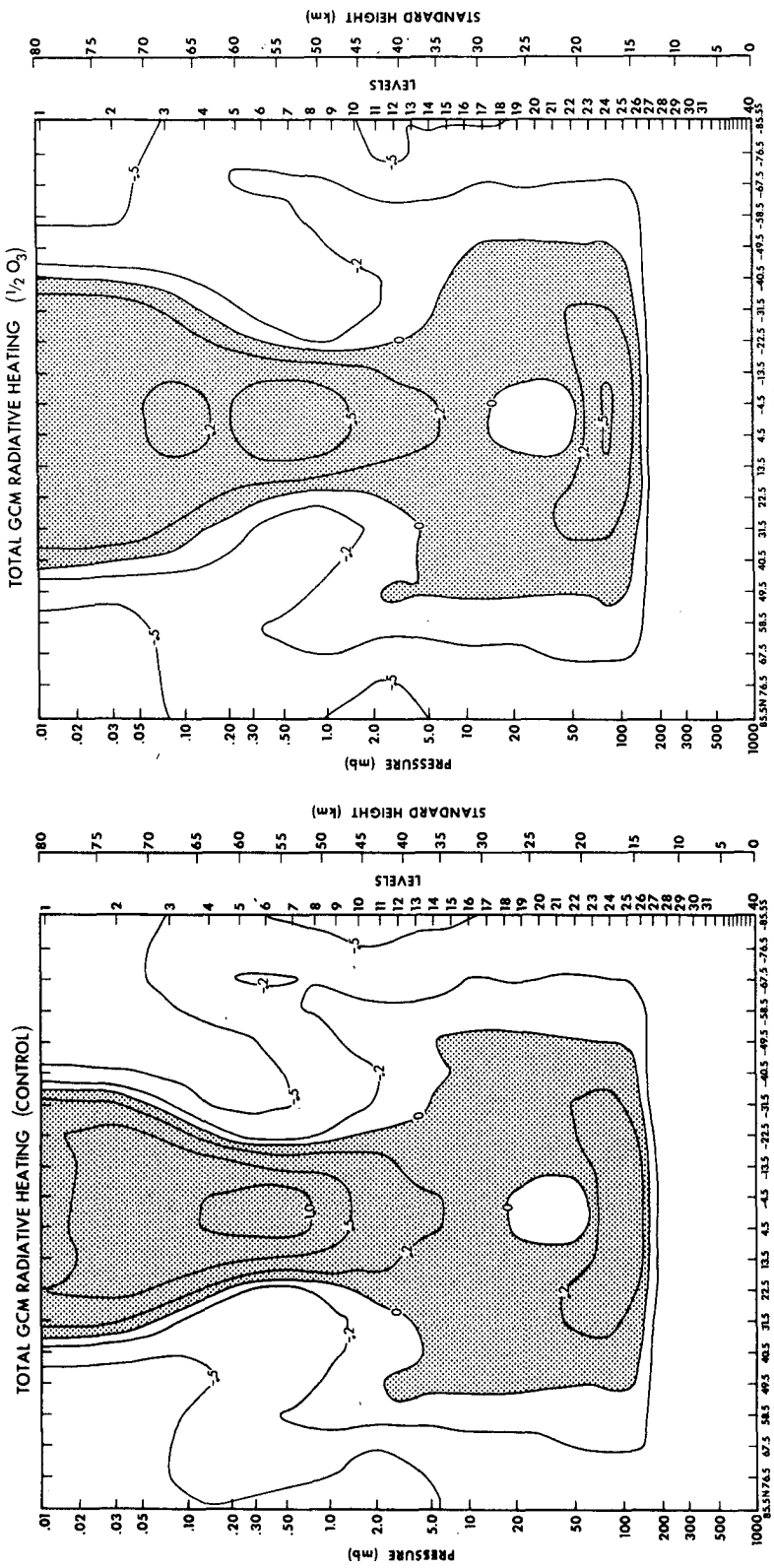

FIG. 5.2. Total radiative heating, $J_{sw} + Q_{lw}$, for (a) the GCM control and (b) the GCM $\frac{1}{2}O_3$ experiments, in units of 10^{-5} K s^{-1}. Regions of radiative heating are shaded.

fested largely through a change in the cooling due to the mean meridional circulation.

Some understanding of why there has been a dynamical adjustment in this portion of the atmosphere can be had by considering the constraints put on the thermal structure by geostrophy. Even though the Coriolis parameter vanishes at the equator, the actual GCM zonal winds in the control experiment (Fig. 5.3a) are in very good agreement with those computed from the GCM control thermal structure and geostrophy (Fig. 5.4a). This verifies that throughout the stratosphere and mesosphere, the zonal-mean temperature field ($\bar{T}$) and zonal wind ($\bar{U}$) are very nearly in geostrophic balance.

In view of this close coupling between $\bar{T}$ and $\bar{U}$, it is of interest to examine the balanced wind field which would exist in the $\frac{1}{2}O_3$ thermal field predicted by the FDH model. It is conceivable, for example, that this predicted $\bar{U}$ might turn out to be dynamically unstable, and this in itself would argue against a purely radiative adjustment.

The geostrophic zonal wind based on the FDH $\frac{1}{2}O_3$ results is shown in Fig. 5.4b, and is striking for the strong easterly core in the tropical mesosphere, and the intense shear zones near 30°. This is a reflection of the sharp reversed meridional temperature gradient predicted by the FDH model. The actual $\frac{1}{2}O_3$ GCM zonal wind shown in Fig. 5.3b has only very weak mesospheric easterlies, and a much milder meridional gradient of $\bar{U}$. The difference between the GCM control and the $\frac{1}{2}O_3$ $\bar{U}$ in the equatorial mesosphere is about -5 m s^{-1}, far less than the -50 m s^{-1} demanded by the FDH model.

As it happens, $\bar{U}$ in the FDH model is on the margin of inertial instability in the tropical mesosphere, with $-\partial\bar{U}/\partial y \approx f \approx 2 \times 10^{-5}$ s^{-1} at 9°N. It is therefore natural to wonder whether this might not be responsible for the very different behavior of the GCM and the FDH model. Indeed in a hypothetical experiment in which we reduce O_3 by more than 50%, such an instability could be relevant. The fact that the actual GCM $\bar{U}$ profile for the $\frac{1}{2}O_3$ run is far from inertial instability, however, suggests that it is not this mechanism which forbids a purely radiative adjustment.

The explanation probably lies in the fact that, in the tropics, the GCM zonal winds seem to be maintained against friction largely by wave-mean flow interaction. It is plausible to expect that the waves, and therefore the zonal flow, will not be drastically changed by altered O_3. For this reason, the wind profile implied by the FDH model is unlikely, and if geostrophy is to be maintained, it is Q_{dyn} which must change.

In this connection, it is interesting to notice that throughout the extratropical mesosphere in both hemispheres, the change in $\bar{U}$ in the GCM due to O_3 reduction is significant (-5 to -10 m s^{-1}), and in fair agreement with the predictions of the FDH model. This suggests that, in these latitudes, it is $\bar{U}$ which has adjusted to the radiatively altered temperature. This difference in the character of the response is not unexpected. In Appendix C we present a simple analytic model which predicts dynamical adjustment to O_3 reduction to be confined to the tropics.

The decrease in the strength of the polar jet shown by our model is similar to that found in the symmetric quasi-geostrophic model of Schoeberl and Strobel (1978). This is quite reasonable, since in this portion of the atmosphere, both models respond radiatively to altered ozone amount. The character of the tropical response in the Schoeberl and Strobel model is difficult to discern in their Fig. 3, but it does appear to be more nearly radiative than in our model.

The other noticeable difference between the GCM and FDH results is in the region just above the tropopause. Careful examination of Figs. 5.1a and 5.1b shows that the FDH model consistently overestimates sensitivities in this region by between 0 and 2 K. The small size of this effect makes its dynamical cause difficult to diagnose. Near the tropical tropopause, however, the difference between the two model sensitivities is substantially more pronounced. To show this comparison in more detail, we have plotted in Fig. 5.5 vertical profiles for the GCM control and $\frac{1}{2}O_3$ temperatures at 4.5°N, along with the corresponding fixed dynamical heating model results for the $\frac{1}{2}O_3$ experiment. The figure shows that the FDH model substantially overestimates the sensitivity at 16 km (level 25) and underestimates it at 19 km (level 23). In view of the probable importance of the tropical tropopause temperature in determining the stratospheric water vapor content, it is useful to analyze this portion of the experiment in some detail. In this connection, it is worthwhile pointing out that the RCE model (Fig. 4.4a) does no better than the FDH model in simulating the GCM response (Fig. 5.1a) in the lower stratosphere. This suggests that the failure of the FDH model in this region is not simply due to neglect of convective processes.

The temperature of the tropical tropopause is determined (in our GCM, at least) by a delicate balance between dynamical *cooling* and longwave *heating* (see also Manabe and Mahlman, 1976). Heating by solar radiation is unimportant in this part of the atmosphere. The longwave heating rate is quite insensitive to temperature changes, so that the local temperature is very sensitive to changes in dynamical heating/cooling. By perturbing the fixed dynamical heating model, we have determined that an increase in dynamical heating of

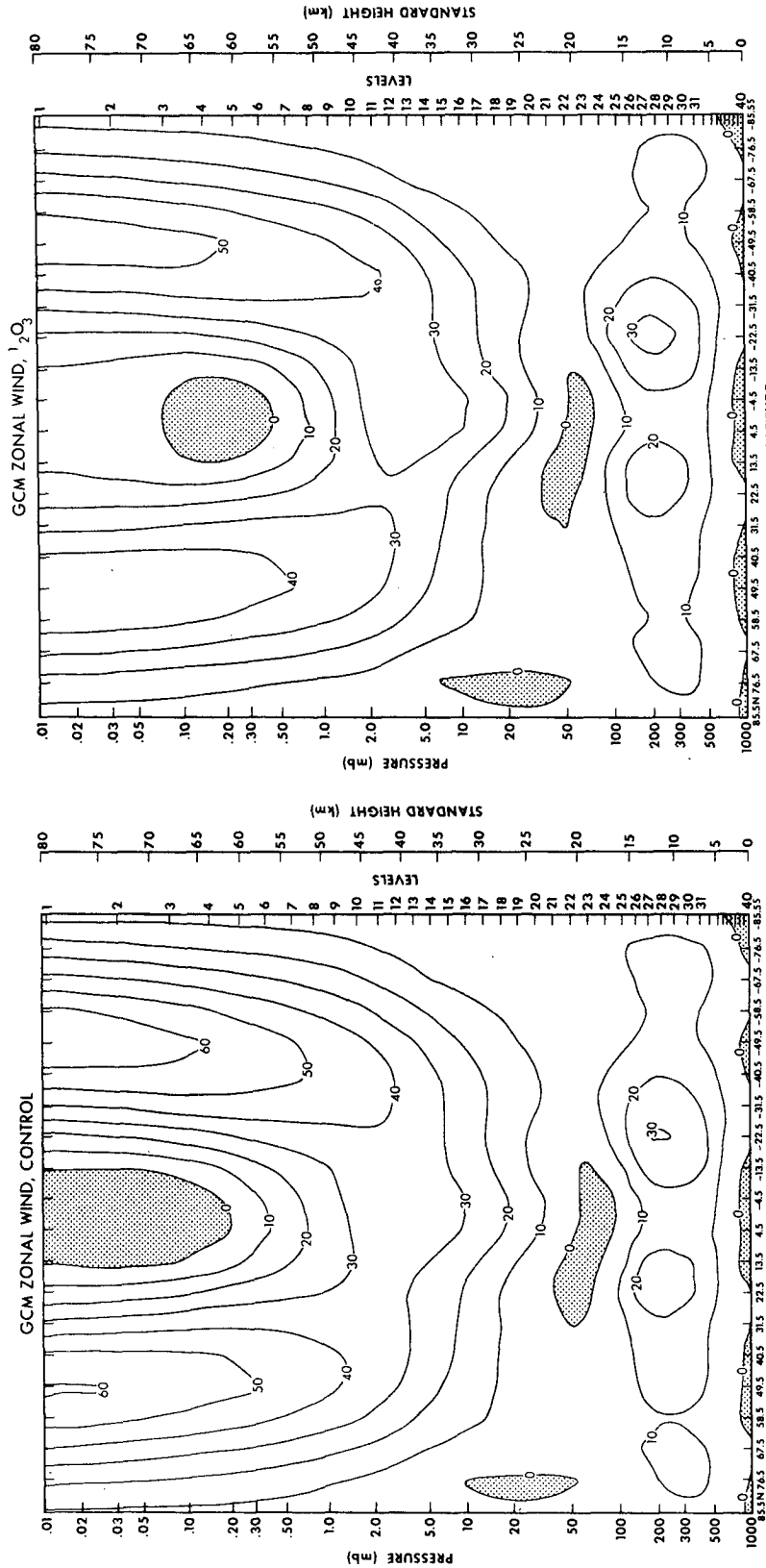

FIG. 5.3. Time-average zonal mean zonal wind ($\bar{U}$) (m s^{-1}) from the GCM (a) control experiment and (b) $^1/_2O_3$ experiment. Regions of easterlies are shaded.

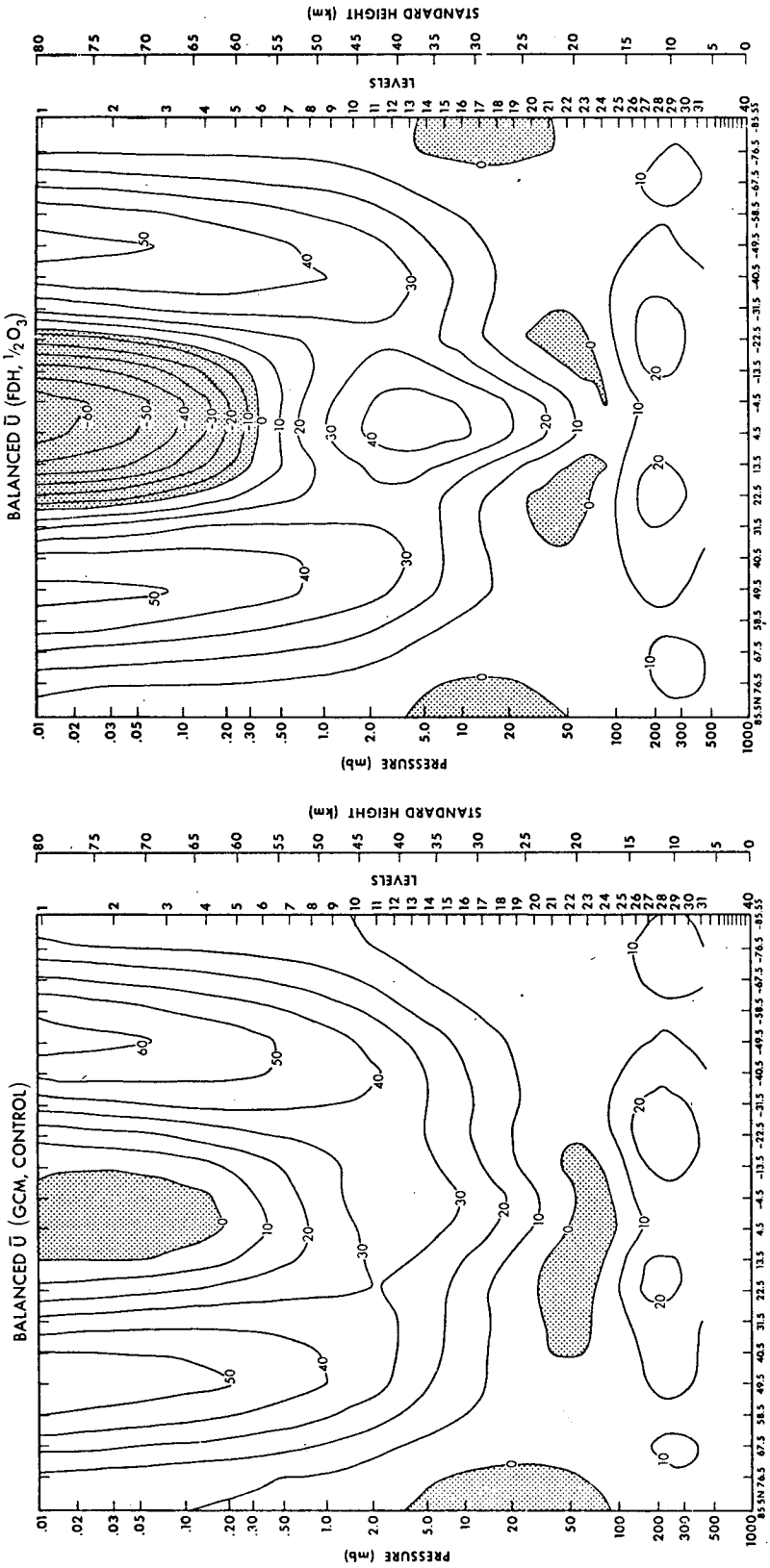

FIG. 5.4. Geostrophically balanced zonal winds ($\bar{U}_{\rm bal}$) computed using (a) the GCM control temperature field and (b) the FDH ½O_3 temperature field. In both cases $\bar{U}_{\rm Bal}$ was calculated by integrating

$$\frac{\partial}{\partial z}(\bar{U}_{\rm bal}) + \frac{\bar{U}^2_{\rm bal}\tan\theta}{af} = -\frac{1}{f}\frac{\partial}{\partial z}\frac{\partial\Phi}{\partial y},$$

and using the actual GCM wind at the lowest level. Here θ is the latitude, a the earth's radius, f the Coriolis parameter and Φ is the geopotential.

0.2 K day^{-1} at 16 km increases the temperature there by 9 K (cf. Fig. B1), while a decrease of 0.2 K day^{-1} lowers the temperature by 13 K. This extraordinary delicacy means that rather small dynamical changes can have a pronounced effect on the temperature.

The balance of heating terms is shown in detail in Table 5.1, which breaks the dynamical terms into several pieces: large-scale dynamics, horizontal diffusion and parameterized vertical transport. To show the character of the data, we have presented results for both 4.5°N and 4.5°S, and used a 120-day averaging period. A crude estimate of the amount of temporal variance in the large scale dynamics term is given in Table 5.1; it was obtained simply by calculating the difference of the heating rates between two separate 60-day averaging periods. The entry labeled "parameterized vertical transport" is the sum of heating due to vertical diffusion and convective adjustment. For technical reasons, there is a substantial amount of cancellation between these two processes.

It is quite clear from Table 5.1 that there have been significant changes in the large-scale dynamical heating due to the ozone reduction, and that these changes are consistent with the changes in the temperature structure. At levels 22, 23 and 24, halving O_3 has resulted in *decreased* dynamical heating, while at levels 25, 26 and 27 there has been an *increase* in dynamical heating. The size of these effects is generally on the order of 0.1–0.2 K day^{-1}, and are larger than those due to the parameterized processes. It is due to these changes that the GCM sensitivity is greater than that of the FDH model at levels 23 and 24, and less at levels 25, 26 and 27.

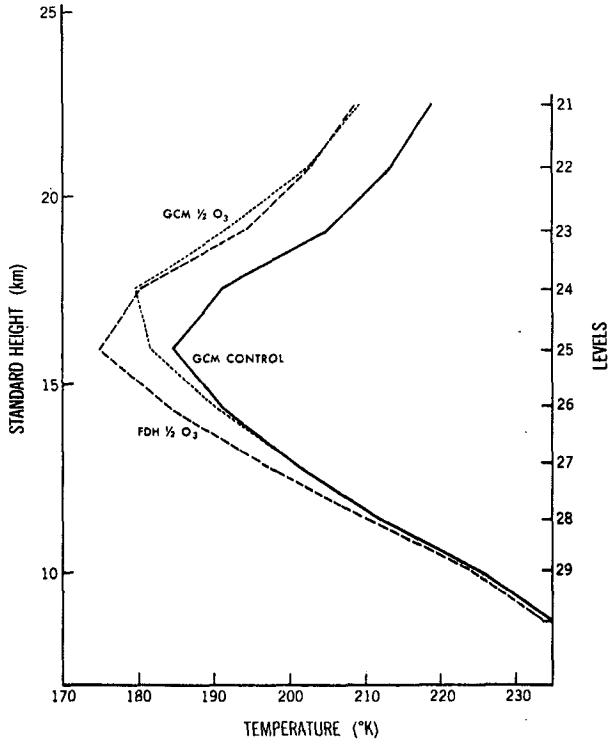

FIG. 5.5. Temperature profile at the tropical latitude, 4.5°N, for the GCM control, GCM ½O_3 and FDH ½O_3 experiments.

The heating due to dynamical processes is con-

TABLE 5.1. Dynamical heating rates at tropical points for control and ½O_3 GCM experiments. All heating rates are in 10^{-5} K s^{-1}, based on 120-day averages. The LSD variance is obtained in Section 5a.

Level	Standard height (km)	Large-scale dynamics (LSD) Control	Large-scale dynamics (LSD) ½O_3	LSD variance	Horizontal diffusion Control	Horizontal diffusion ½O_3	Parameterized vertical transport* Control	Parameterized vertical transport* ½O_3
				4.5°N				
22	20.9	0.205	0.155	0.030	−0.045	−0.051	0.000	−0.001
23	19.2	0.027	−0.230	0.045	−0.043	−0.003	0.000	−0.007
24	17.5	−0.424	−0.617	0.084	0.034	0.126	0.014	−0.018
25	16.0	−0.570	−0.409	0.000	0.114	0.089	−0.021	0.015
26	14.4	−0.325	−0.221	0.008	0.063	0.051	0.031	0.047
27	12.9	−0.019	0.072	0.013	0.051	−0.001	0.117	0.205
28	11.4	0.038	0.143	0.004	0.022	−0.042	0.895	0.920
				4.5°S				
22	20.9	0.193	0.107	0.021	−0.050	−0.056	0.001	0.000
23	19.2	0.049	−0.235	0.025	−0.036	−0.018	−0.001	−0.003
24	17.5	−0.456	−0.582	0.067	0.059	0.110	−0.023	−0.051
25	16.0	−0.578	−0.435	0.018	0.140	0.135	−0.039	−0.060
26	14.4	−0.374	−0.249	0.005	0.126	0.107	0.007	−0.029
27	12.9	−0.052	0.039	0.000	0.067	0.086	0.119	0.135
28	11.4	0.032	0.076	0.020	0.003	0.038	0.919	0.908

* Vertical diffusion plus convective adjustment.

TABLE 5.2. Large-scale dynamical heating rates in the tropics broken into mean meridional and eddy components. All heating rates are in 10^{-5} K s^{-1}, based on 120-day averages.

Level	Standard height (km)	Mean meridional circulation		Eddy circulation	
		Control	½O_3	Control	½O_3
		4.5°N			
22	20.9	0.261	0.201	−0.056	−0.047
23	19.2	0.272	0.190	−0.245	−0.420
24	17.5	0.203	0.116	−0.626	−0.732
25	16.0	0.078	−0.073	−0.648	−0.337
26	14.4	−0.120	−0.308	−0.205	0.087
27	12.9	−0.253	−0.410	0.234	0.483
28	11.4	−0.197	−0.273	0.236	0.415
		4.5°S			
22	20.9	0.284	0.274	−0.091	−0.167
23	19.2	0.298	0.230	−0.248	−0.465
24	17.5	0.183	0.120	−0.638	−0.702
25	16.0	0.031	−0.030	−0.609	−0.405
26	14.4	−0.127	−0.151	−0.247	−0.098
27	12.9	−0.183	−0.156	0.132	0.195
28	11.4	−0.105	−0.082	0.137	0.159

ventionally divided into a portion due to the mean meridional circulation, and one due to eddies. It has been pointed out, however, that this may be quite misleading, due to existence of "induced" meridional circulations which can be produced by the eddies themselves (Dickinson, 1969). In spite of this caveat, we think it interesting to present the results of such a decomposition, and this is done in Table 5.2.

The results of this decomposition suggest strongly that changes in the eddy processes are responsible for the altered dynamical heating rates; certainly a perusal of the heating rate changes shows that changes in the eddy term are always of the correct sign. At levels 23 and 24, changes in the mean circulation heating act in concert with changes in the eddy heating, while at levels 25, 26 and 27 the two act in opposition. It is therefore not possible without more sophisticated analysis to determine precisely what is cause and what is effect; nevertheless, the fact that there *are* changes in the eddy heating suggests that a coupling of the sort described in Section 4a may be at work here. There are several possible causes of changes in the dynamical heating in this region—the alteration of static stability and of zonal wind structure are obvious candidates. The most dramatic changes have taken place at the equator as previously mentioned, but there has been a general weakening of the westerlies in midlatitudes. It is also worth noting the region of increased westerlies near the tropical tropopause. Whether any of these changes can account for the altered heating is a question which we still have not addressed.

2) CHANGE IN WATER VAPOR

In the middle and upper stratosphere, the residence time of water vapor is many years, substantially longer than the integration period in this experiment. Therefore, although the GCM has a carefully constructed advection scheme for trace constituents, the lack of equilibrium makes a full discussion of the effect of changed O_3 on water vapor amounts impossible. In the lower stratosphere, however, response times are shorter, and there are clear indications that the reduced temperatures have had a desiccating effect. At 16 km in the tropics, for example, the mixing ratio has dropped from 0.4 to 0.2×10^{-6} kg kg^{-1}, the relative humidity there remaining approximately constant at ~50%. In midlatitudes at the same height, there is a similar but smaller decrease (0.8 to 0.6×10^{-6} kg kg^{-1}). These very low tropical mixing ratios in the control experiment are associated with the relatively low temperature at the tropical tropopause.

b. Response to carbon dioxide increase

There are no important differences between the δT found from the FDH model (Fig. 5.6a) and that of the GCM (Fig. 5.6b), showing that the dynamical heating has remained effectively constant. In the upper stratosphere and mesosphere the similarity is particularly striking. In the lower stratosphere there are noticeable differences on the order of ~1 K or less: the region of positive δT between 10 and 13 km, in the polar region, is absent in the FDH model. The temperature of the tropical tropopause in the GCM has risen by ~0.5 K, while the FDH model predicts an increase of ~1.5 K there. Although these are real effects, their very small size makes them relatively uninteresting.

In view of the remarkable flatness of the FDH thermal response in the middle atmosphere and the very small changes in static stability near the tropopause, it is perhaps not surprising that the dynamical heating has remained so steady. On the other hand, one might have expected that changes in the CO_2 amount might have affected the radiative damping of stratospheric waves, and therefore their dynamics. By perturbing the radiative equilibrium model and observing the subsequent temporal behavior, it is possible to study the thermal relaxation times (τ^{rad}) and their change when CO_2 is increased. We find that for a perturbation whose scale is 5 km, τ^{rad} = 3.1 days at 75 km and 2.6 days at 45 km. When we double the CO_2 amount these decrease to 2.8 and 2.1 days, respectively. If these changes are important, they can be expected

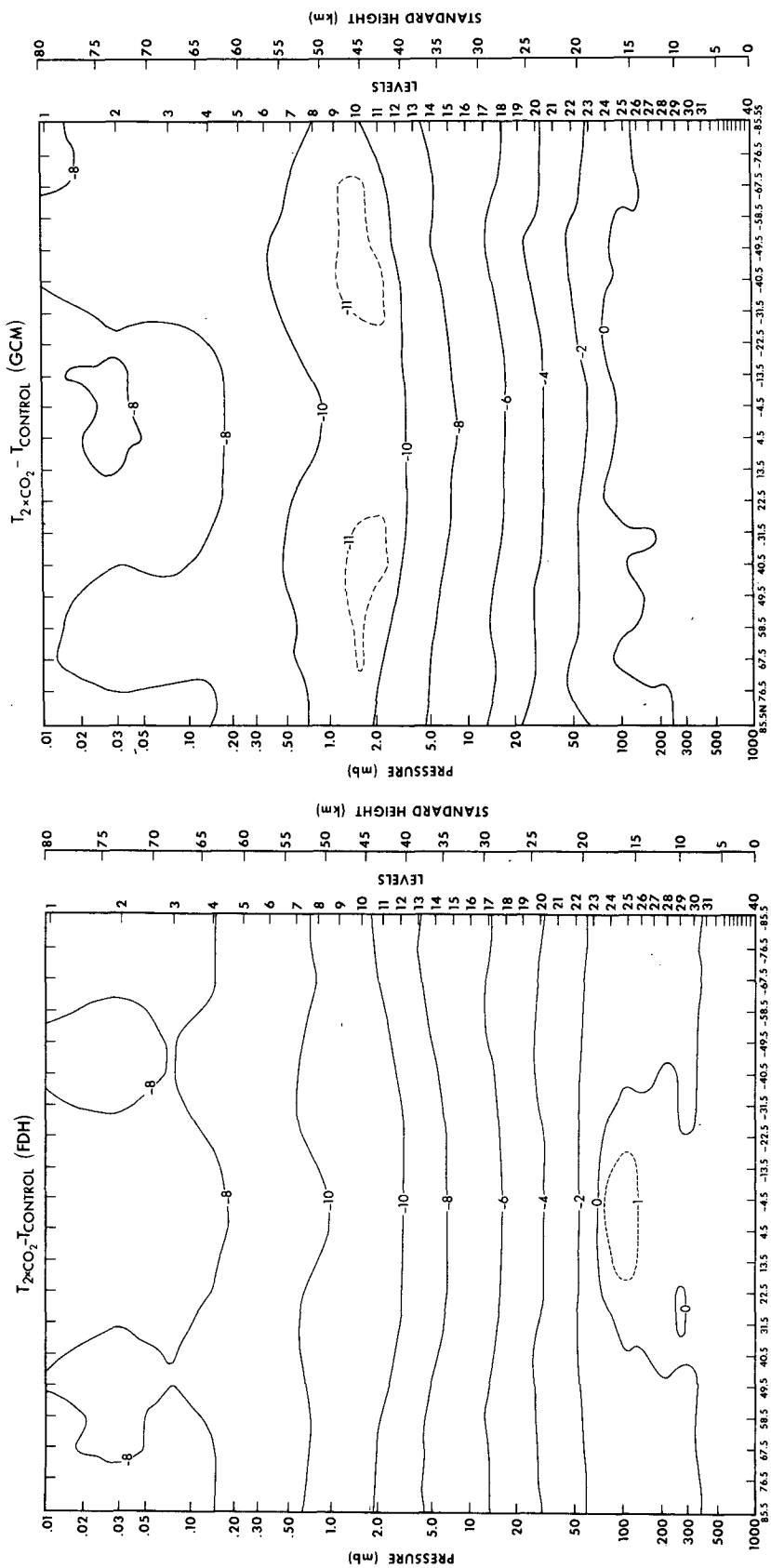

FIG. 5.6. Temperature change due to doubled CO_2 as simulated by (a) the FDH model and (b) the GCM.

to alter the energetics of the wave field. We have therefore examined several quantities relating to wave activity: the eddy kinetic energy, the eddy geopotential flux and the eddy conversion. There are no differences between the control and $2 \times CO_2$ cases for any of these quantities which cannot be attributed to statistical fluctuations. Apparently, the changes in damping rates have not noticeably altered the wave dynamics.

6. Conclusions

For the annual mean insolation considered in this paper, the thermal response of the middle atmosphere to changes in O_3 or CO_2 is largely radiative. The dynamical heating is not significantly altered in most of the atmosphere. In view of this, it appears that correctly formulated 2D radiative models are useful tools for the study of stratospheric sensitivity problems. They might profitably be applied to similar problems such as seasonal sensitivity effects and the influence of other gases, such as CFM's.

However, there are two exceptions to the rule that the response is dominantly radiative, both occurring in the ozone-reduction experiment. The tropical mesospheric circulation is altered, due to the changed horizontal gradient in heating. This is consistent with the results of a simple linear dynamical model, which predicts that changes in the dynamical heating due to altered mean meridional circulation will be confined to the tropics. In the tropical lower stratosphere, dynamical heating has also changed, apparently due to altered wave activity there. In this region, therefore, there is some suggestion that the feedback mechanism suggested by Dickinson and others may be at work.

The insensitivity of the doubled CO_2 results to various model assumptions, the absence of important dynamical changes, and the chemical inertness of CO_2, all suggest that the model stratospheric response has captured the essence of what would happen in the real atmosphere. In the O_3 reduction experiment, however, there are several factors which counsel extreme caution in interpreting the results.

In the first place, the assumption of a uniform 50% ozone reduction is unrealistic; related to this is the fact that the present study has evaded a most interesting coupling—the effect of dynamics on ozone distribution. The importance of ozone in determining the thermal structure of the lower stratosphere is an obvious result of the present study, and the central role played by dynamical processes in the distribution of ozone in that part of the atmosphere is well established. Our results hint at the possibility that in the tropical lower stratosphere, important changes in wave activity have occurred. Such changes in a model with interactive (rather than specified) ozone could conceivably further alter the ozone distribution.

Although far from equilibration, our model already shows the lower stratosphere water mixing ratio to have changed in response to changed ozone. In that the chemistry of ozone may be importantly affected by water, this suggests the important future role of fully interactive dynamical-radiative-chemical models in the investigation of stratospheric effects involving altered ozone levels.

Acknowledgments. We have profited greatly from the comments of Drs. I. Held and S. Manabe, and Mr. R. Wetherald on an early draft of this work. Their careful consideration of many questions of exposition and content was invaluable. We are indebted to Drs. R. E. Dickinson and C. Leovy for their perceptive reviews of the manuscript. Ms. J. Kennedy typed the difficult manuscript with great skill and speed. Mr. P. Tunison prepared the figures. We gratefully thank all of them.

APPENDIX A

Parameterization of Radiative-Photochemical Damping

1. Introduction

In the text we point out that the model includes a crude parameterization of the effect of ozone photochemistry on the damping of temperature perturbations in the upper stratosphere beyond that provided by IR radiative transfer (e.g., Leovy, 1964; Lindzen and Goody, 1965; Blake and Lindzen, 1973). This effect is due to the temperature dependence of several important kinetic reactions in the chemistry of O_3. Its essence is that a dynamically induced temperature increase leads to an O_3 decrease. This in turn leads to a decreased O_3 absorption in the ultraviolet, thus decreasing the temperature and damping the original perturbation. The opposite occurs for temperature decreases, again producing a damping effect.

To incorporate this process directly in a GCM, a self-consistent ozone chemistry is required. We have chosen to sidestep this difficult problem by including in the model a simple parameterization of the damping process. In this scheme, a set of ozone mixing ratios is prespecified as a function of latitude and height, as described in Section 2. From these, a radiative-convective equilibrium thermal structure is calculated. In any actual model run, deviations from those calculated temperatures result in modifications to the prespecified ozone.

Before explaining the scheme in detail, several general remarks are useful. It should first be noticed that the parameterization does not significantly alter

the time-mean lower latitude ozone amount in either the RCE or the GCM control experiments. For the RCE case, this is obvious. In the GCM control case, the difference between the GCM temperatures and those of the RCE model above 35 km is small (cf. Figs. 3.1b and 4.3), so that there is little perturbation to the prespecified ozone.

In the $\frac{1}{2}O_3$ experiments, the equilibrium temperatures used in the parameterization are those calculated from a set of $\frac{1}{2}O_3$ radiative-convective equilibria. In doing this, the assumption has been made that the unspecified chemical cause of the ozone reduction has been such as to reduce O_3 uniformly by 50%. Since non-radiative processes do not produce large departures from the equilibrium temperatures, it follows that the damping parameterization does not appreciably change the $\frac{1}{2}O_3$ mixing ratio from its prespecified value.

2. Description of the scheme

We begin by considering a "chemistry only" continuity equation for "odd oxygen" ($N_O + N_{O_3}$), i.e.,

$$\frac{\partial}{\partial t}(N_O + N_{O_3}) = 2N_{O_2}J_{O_2} - 2k_{13}N_O N_{O_3} + \text{"non-Chapman loss"}, \quad \text{(A1)}$$

where N_i is the number density for the indicated constituent, J_{O_2} the photodissociation efficiency for molecular oxygen and k_{13} the rate coefficient for the Chapman loss reaction $O + O_3 \xrightarrow{k_{13}} 2\ O_2$ with a value $1.33 \times 10^{-11} \exp(-2100/T)$ cm^3 molecule^{-1} s^{-1}.

We next evade virtually all of the chemistry by assuming that

$$\text{non-Chapman loss} \approx 2k_{\text{fudge}}N_O N_{O_3}, \quad \text{(A2)}$$

with k_{fudge} defined as

$$k_{\text{fudge}} = 4\bar{k}_{13} = 4 * 1.33 \times 10^{-11} \times \exp(-2100/T_{\text{mean}}) \text{ cm}^3 \text{ molecule}^{-1} \text{ s}^{-1}. \quad \text{(A3)}$$

This simply means we have assumed that the non-Chapman ozone loss is four times the average loss in the region typified by the typical upper stratospheric temperature T_{mean}. Note also that once T_{mean} is prescribed, k_{fudge} is independent of temperature. This appears to be reasonable for the upper stratosphere where the actual non-Chapman ozone loss processes are dominated by HO_x and Cl_x chemistry. The value of 4 for the relative non-Chapman loss efficiency is roughly in agreement with photochemical requirements to give the proper ozone amount in the upper stratosphere. The photochemical model is the one used in Mahlman *et al.* (1980).

At local photochemical equilibrium, we combine (A1) and (A2) to obtain

$$N_{O_3}(T) = \frac{J_{O_2}(T)N_{O_2}(T)}{[k_{13}(T) + k_{\text{fudge}}]N_O(T)}. \quad \text{(A4)}$$

At least up to the lower mesosphere, the ratio of O to O_3 can be assumed to adjust instantaneously. This is equivalent to saying that the photodissociation of O_3

$$O_3 + h\nu \xrightarrow{J_{O_3}} O_2 + O \quad \text{(A5)}$$

and the three-body recombination

$$O + O_2 + M \xrightarrow{k_{12}} O_3 + M \quad \text{(A6)}$$

occur very fast relative to the odd oxygen destruction processes. [Here we define $k_{12} = 2.04 \times 10^{-35} \times \exp(1050/T)$ cm^6 molecules^{-2} s^{-1}.] This statement of balance is

$$k_{12}N_O N_{O_2} N_m = J_{O_3}N_{O_3}. \quad \text{(A7)}$$

Eq. (A7) can then be substituted into (A4) to eliminate N_O and obtain

$$N_{O_3}(T) = 0.209N_m^{3/2}\left[\frac{J_{O_2}(T)k_{12}(T)}{J_{O_3}(T)[k_{13}(T) + k_{\text{fudge}}]}\right]^{1/2}. \quad \text{(A8)}$$

Equivalently, we can express Eq. (A8) in terms of *mass* mixing ratio

$$R_{O_3}(T) = 1.657N_{O_3}(T)N_m^{-1}. \quad \text{(A9)}$$

The above equations are not applicable at all altitudes. Below ~34 km the odd oxygen production efficiency becomes slow relative to transport effects. Above ~65 km, the three-body reaction of Eq. (A6) becomes slow enough that the ratio of O to O_3 may differ significantly from equilibrium.

In the GCM the prescribed ozone (which gives the correct temperature) is assumed to be that of the control radiative-photochemical equilibrium state $[R_{O_3}(T_{eq})]$. The correction to that equilibrium ozone would be

$$R_{O_3}(T) \equiv R_{O_3}(T_{eq})\frac{R_{O_3}(T)}{R_{O_3}(T_{eq})}. \quad \text{(A10)}$$

This identity gives us a formula for calculating the deviation of ozone from its prescribed value. We simply evaluate Eq. (A9) substituted into (A8) in the form of the ratio

$$\frac{R_{O_3}(T)}{R_{O_3}(T_{eq})} \equiv D = \left[\frac{\dfrac{J_{O_2}(T)k_{12}(T)}{J_{O_3}(T)[k_{13}(T) + k_{\text{fudge}}]}}{\dfrac{J_{O_2}(T_{eq})k_{12}(T_{eq})}{J_{O_3}(T_{eq})[k_{13}(T_{eq}) + k_{\text{fudge}}]}}\right]^{1/2}. \quad \text{(A11)}$$

We assume that the ratio of the J's is less sensitive

to temperature perturbations than are the ratios of the k's. This is clearly true for local temperature fluctuations. For shifts of the entire column, the approximation can become highly questionable (Strobel, 1977; Hartmann, 1978). Nevertheless, for simplicity we assume it is so. Substituting in the values for the k's defined above, Eq. (A11) becomes

$$D \approx \left[\exp(1050/T - 1050/T_{eq}) \times \frac{4\exp(-2100/T_{mean}) + \exp(-2100/T_{eq})}{4\exp(-2100/T_{mean}) + \exp(-2100/T)}\right]^{1/2}, \quad \text{(A12)}$$

where $T_{mean} = 265$ K.

For the GCM, the values of T_{eq} as well as $R_{O_3}(T_{eq})$ are required. Using Eqs. (A10), (A11) and (A12) the altered local photochemical equilibrium GCM ozone is simply

$$R_{O_3}(T) = R_{O_3}(T_{eq})*D. \quad \text{(A13)}$$

These altered values of ozone mixing ratio are then used in the GCM radiation algorithms in calculating heating rates.

This parameterization appears to work reasonably well in lower latitudes. In higher latitudes, the approximations tend to break down. However, the damping effect of this process is considerably weakened there because of the lack of local solar heating. As an extreme example, in the polar night the value of D becomes meaningless physically. However, no shortwave ozone heating is occurring there anyway.

3. Application to the 2 × CO_2 and ½O_3 experiments

For the 2 × CO_2 experiment the temperature departure from radiative-photochemical equilibrium is calculated from the *old* control radiative-photochemical equilibrium. We assume that the amount of non-Chapman ozone destroying material has not changed in the 2 × CO_2 atmosphere, although it is not obvious that this would be so if CO_2 really were to double. Thus, as the stratosphere cools in response to the increased CO_2, its ozone (from 34 to 80 km) increases as specified in the radiative-photochemical parameterization scheme.

For the ½O_3 experiment, a more complex procedure is required. Because the ozone has been reduced by a factor of 2 everywhere, it is necessary to ascribe a chemical "cause" for the drastic decrease. In this experiment, we assume that the entire decrease occurs due to temperature-*independent* non-Chapman reactions. This has the physical effect of decreasing the efficiency of the radiative-photochemical damping mechanism relative to the control. This is because the contribution due to the Chapman ozone loss is masked by the larger non-Chapman loss.

Using the same logic leading to Eq. (A11) and its approximate form of Eq. (A12), we can calculate

$$2 = \frac{R_{O_3}(T_{eq})}{R_{O_3}(T'_{eq})} \approx \left[\frac{\dfrac{k_{12}(T_{eq})}{k_{13}(T_{eq}) + 4\bar{k}_{13}}}{\dfrac{k_{12}(T'_{eq})}{k_{13}(T'_{eq}) + X\bar{k}_{13}}}\right]^{1/2}, \quad \text{(A14)}$$

where X is the ratio of non-Chapman loss to Chapman loss required to reduce the equilibrium ozone by the indicated factor or 2, and T'_{eq} is the ½O_3 radiative-photochemical equilibrium temperature. Solving for X, we obtain $X = 22.7$. Inspection of Eq. (A12) (with 4 replaced by 22.7) shows that the remaining temperature dependence on the ozone amount is due almost completely to the 3-body recombination of Eq. (A6).

APPENDIX B

Details of Radiative Response to Altered Composition

The basic transfer equation for IR heating/cooling due to a single spectral band (such as the CO_2 15 μm complex) can be written as

$$Q_{lw}(p) = \frac{g}{c_p}\left\{B_\nu(T^*)\frac{\partial\tau}{\partial p}(p, p^*) - \int_0^{p^*} B_\nu(p')\frac{\partial^2\tau}{\partial p\partial p'}(p, p')dp'\right\}. \quad \text{(B1)}$$

Here B_ν is the Planck function at band center ν, evaluated at temperature $T(p)$; $\tau(p, p')$ is the broadband transmission function; and T^* and p^* are the surface temperature and pressure. At equilibrium, therefore, we have

$$J_{sw} + Q_{dyn} + \frac{g}{c_p}\left\{B_\nu(T^*)\frac{\partial\tau}{\partial p}(p, p^*) - \int_0^{p^*} B_\nu(p')\frac{\partial^2\tau}{\partial p\partial p'}(p, p')dp'\right\} = 0. \quad \text{(B2)}$$

1. Changes induced by altered O_3 amount

In the O_3 reduction experiment, we change J_{sw} by perturbing the ozone mixing ratio. We also alter the heating rates due to the 9.6 μm ozone IR band, but we will ignore this effect for the moment. Since we assume the adjustment to be purely radiative, the induced temperature change is given implicitly by the integral equation

$$\delta J_{sw} + \frac{g}{c_p}\left\{\delta B_\nu(T^*)\frac{\partial\tau}{\partial p}(p, p^*) - \int_0^{p^*}\delta B_\nu(p')\frac{\partial^2\tau}{\partial p\partial p'}dp'\right\} = 0. \quad \text{(B3)}$$

In principle, the above equation can be inverted to give

$$\delta B_\nu(p) = \int_0^{p^*} K(p, p')\delta J_{sw}(p')dp'. \quad \text{(B4)}$$

The influence function $K(p, p')$ is a measure of the effect of a change in the heating at p' on the temperature at p. For any finite-difference version of (B3), there also exists a discrete analogue of (B4). In Fig. B1 we display part of the influence matrix appropriate to our finite difference mesh. It is worth noting that effects due to a perturbation in J_{sw} are rather well localized, so that it is usually possible to understand induced temperature changes as simple responses to local changes in heating.

The local change in heating δJ_{sw} due to a 50% reduction in O_3 is shown in Fig. 4.1a. The general structure is straightforward; there is a maximum at all latitudes near 55 km, and a pronounced meridional gradient, with the largest changes in the tropics. Between ~40 and 22 km, δJ_{sw} is <1 K day^{-1} and decreases poleward, but between 22 and 15 km, the larger changes are in the polar region.

Most of this behavior can be understood by consideration of a simple model in which the strongly absorbing Hartley-Huggins complex is modeled as a gray absorber with coefficient k_H, and the very weak Chappuis bands (which are always in the optically thin regime) by k_C, so that

$$J_{sw} \propto \mu^{-1}R_{O_3}\left\{\mu I_C k_C + \mu I_H \times \exp\left[-k_H\mu^{-1}\int_0^p R_{O_3}\frac{dp'}{g}\right]\right\}. \quad \text{(B5)}$$

R_{O_3} is the ozone mixing ratio, μ the cosine of the zenith angle and the intensities I_C and I_H are constant.

Reduction of ozone by 50% always leads to a 50% reduction in the Chappuis term; in those regions where

$$\mu^{-1}\int_0^p k_H R_{O_3}dp'/g \ll 1,$$

reduction of R_{O_3} also decreases the Hartley-Huggins heating. Deeper in the atmosphere, however, reduction of R_{O_3} actually *increases* this term. This cross-over point lies higher in the atmosphere in the polar regions due to the larger value of μ. This explains the very sharp vertical and meridional gradients near 40 km. In the lower stratosphere, most of the heating is due to the weakly absorbed component, which, being proportional to R_{O_3}, is larger at the poles than in the tropics.

For the 15 μm band of CO_2, $B_\nu(T) \propto e^{-960/T}$, so that Eq. (B4) may be written in terms of δT as

$$\delta T(p) \propto T^2 e^{960/T}\int_0^{p^*} K(p, p')\delta J_{sw}(p')dp'. \quad \text{(B6)}$$

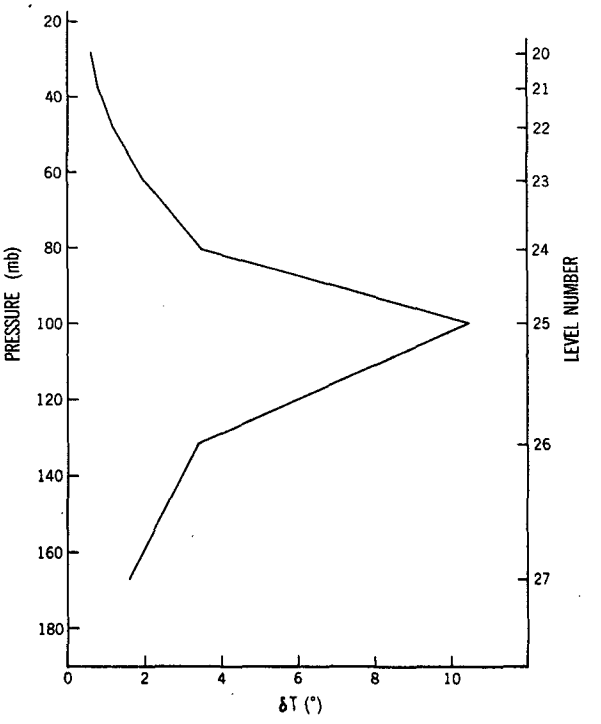

FIG. B1. Change in equilibrium temperature at various levels produced by a 0.2 K day^{-1} change in the heating at level 25 (16 km). The approximate locality of the response is evident.

The function $T^2e^{960/T}$ drops by almost a factor of 4 between 170 and 300 K, so that for a given δJ_{sw}, the resultant temperature change depends in an important way on the assumed unperturbed temperature. If the latter is too cold, we will overestimate δT, and if too warm, underestimate it.

Effects due to changes in 9.6 μm heating rates can be estimated by using Eq. (B2) to evaluate the change in O_3 IR heating rates, assuming that the thermal structure does not change; i.e., by assuming that

$$\delta Q_{9.6} \approx \left\{B_\nu(T^*)\delta\left(\frac{\partial\tau}{\partial p}\right)_{9.6} - \int_0^{p^*}\delta\left(\frac{\partial^2\tau}{\partial p\partial p'}\right)_{9.6}B_\nu(p')dp'\right\}. \quad \text{(B7)}$$

For an optically thin gas, $\delta(\partial\tau/\partial p)$ is proportional to $(\partial\tau/\partial p)$ so that we expect that reduction in ozone by 50% should yield about a 50% reduction in $Q_{9.6}$. In Fig. B2, we display $Q_{9.6}$ for the standard ozone distribution; $\delta Q_{9.6}$ due to a 50% reduction of ozone is shown in Fig. 4.1b. For approximate purposes, $\delta Q_{9.6}$ may be added to the change in shortwave heating to predict the change in thermal structure. Figs. 4.1a and 4.2b show that the effect is to decrease the change in temperature in the upper stratosphere, where $Q_{9.6}$ is negative, and to increase

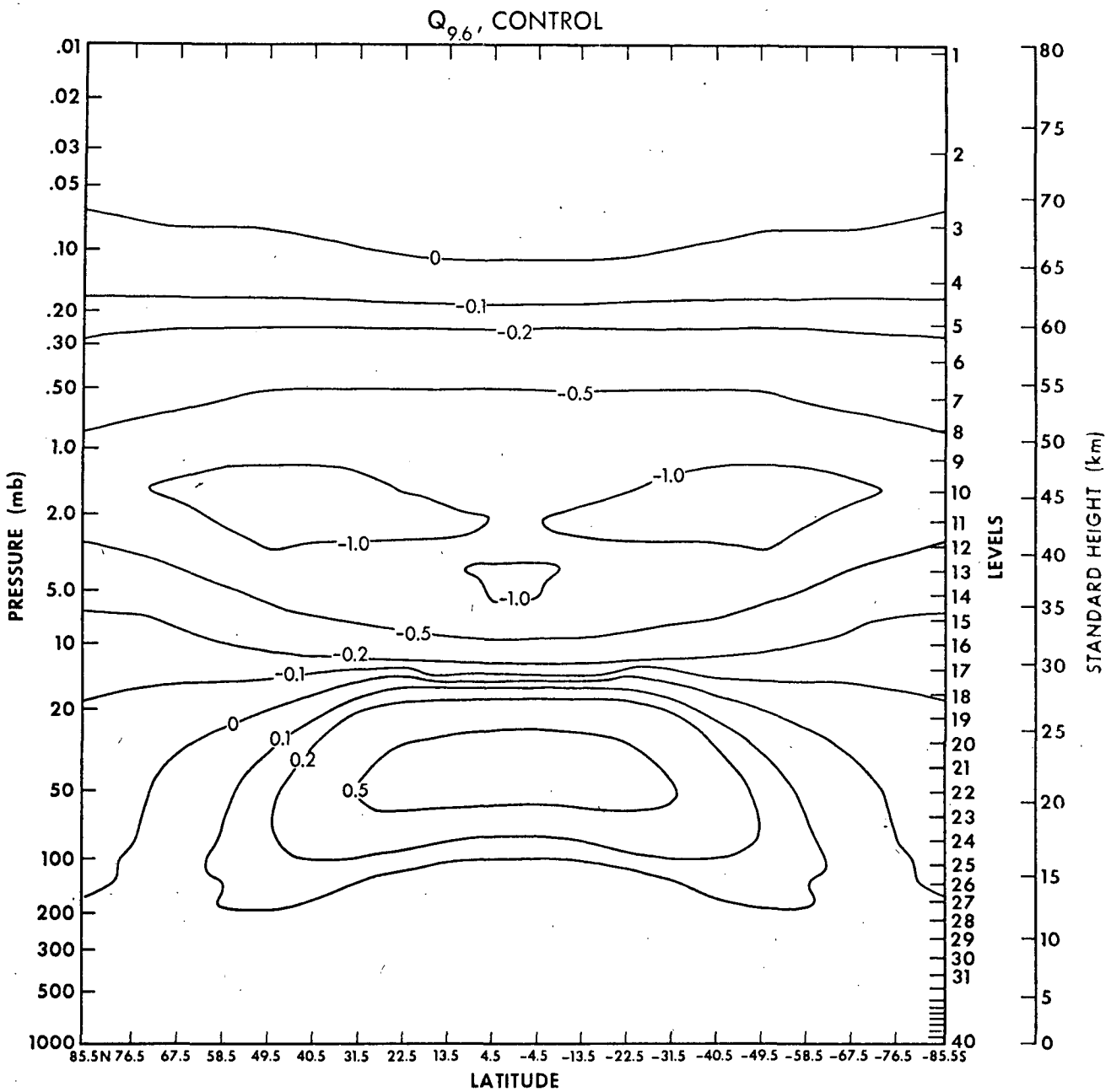

FIG. B2. Radiative heating rate ($Q_{9.6}$) for the 9.6 μm O_3 band (K day^{-1}) using the GCM control mixing ratios and temperatures.

it in the tropical lower stratosphere, where $Q_{9.6}$ is positive. It is interesting that between 22 and 16 km in the tropics, the 9.6 μm effect is larger than the local shortwave effect.

The exact values of $Q_{9.6}$ obviously depend on the basic thermal state assumed, and on the distribution of high clouds. In general, colder stratospheric temperature leads to larger values for $Q_{9.6}$, while more high clouds reduce $Q_{9.6}$. The results discussed above correspond to the temperature field shown in Fig. 3.1b, and to a 21% tropical cirrus cover. When the cirrus amount is doubled one finds that $Q_{9.6}$ in the lower stratosphere is reduced by about two thirds.

2. Changes induced by altered CO_2 amount

When the carbon dioxide mixing ratio is increased, the effects depend strongly on altitude. Above ~30 km, the local effect dominates; more radiating molecules lead to increased cooling, and therefore lowered temperature. In the lower stratosphere, however, the increased optical path

between the layer in question and space is the dominant change, and this leads to a decrease in cooling rate.

These remarks can be made somewhat more precise by considering Eq. (B2) as it models the response to altered CO_2 amount; since in this case Q_{dyn} and J_{sw} are unchanged, we have[13]

$$0 = \delta Q_{lw}$$

$$= \left[B_\nu^*(T^*)\delta\left(\frac{\partial\tau}{\partial p}\right) - \int_0^{p^*} B_\nu(p')\delta\left(\frac{\partial^2\tau}{\partial p\partial p'}\right)dp' \right]$$

$$+ \left\{ \delta B_\nu^*(T^*)\frac{\partial\tau'}{\partial p} - \int_0^{p^*} \delta B_\nu(p')\frac{\partial^2\tau'}{\partial p\partial p'}\,dp' \right\}. \quad \text{(B8)}$$

The first terms (in square brackets) represent the change in longwave cooling due to changed CO_2 mixing ratio at a given temperature; the second pair of terms (in braces) is the change in the cooling rate due to altered temperature. It is obvious that the required δB_ν will be that derived from an effective change in heating given by

$$(\delta J)_{\text{eff}} = \frac{g}{c_p}\left\{ B_\nu^*\delta\left[\frac{\partial\tau}{\partial p}(p, p^*)\right] - \int_0^{p^*} B_\nu(p')\delta\left[\frac{\partial^2\tau}{\partial p\partial p'}\right]dp' \right\}. \quad \text{(B9)}$$

Although $(\delta J)_{\text{eff}}$ depends on the assumed unperturbed thermal structure, certain general properties can be deduced by considering a random model for CO_2 absorption, and calculating the Q_{lw} in the cool-to-space approximation. In this case, Q_{lw} is proportional to $\partial\tau(o, p)/\partial p$, and $\tau(o, p) = \exp(-c'p)$; c' is a constant which depends on the CO_2 mixing ratio. With these approximations, Q_{lw} is proportional to $-c'e^{-c'p}$, and $(\delta J)_{\text{eff}}$ to $e^{-c'p}\delta c'[-1 + c'p]$. For small values of p, therefore, $(\delta J)_{\text{eff}}$ is negative and relatively large; for $c'p > 1$, however, it becomes positive and very small.

In Fig. 4.2a we exhibit $(\delta J)_{\text{eff}}$ for the $2 \times CO_2$ case, based on the thermal profile shown in Fig. 3.1b; the behavior is as predicted above.

3. Comparison of the ½O_3 and $2 \times CO_2$ forcing

As discussed above, the effective forcing for δT in the ½O_3 case is $\delta J_{sw} + \delta Q_{9.6}$, while in the $2 \times CO_2$ case it is $(\delta J)_{\text{eff}}$; these are compared in Fig. 4.2. Several important differences between the two drives are obvious: 1) The magnitude as well as the meridional gradient of $\delta J_{sw} + \delta Q_{9.6}$ is substantially larger at 55 km than that of $(\delta J)_{\text{eff}}$; 2) the vertical gradient of $\delta J_{sw} + \delta Q_{9.6}$ around 45 km is much larger than that of $(\delta J)_{\text{eff}}$; 3) between 16 and 20 km, $\delta J_{sw} + \delta Q_{9.6}$ is substantially more negative than $(\delta J)_{\text{eff}}$. In fact, the latter is actually positive near the tropical tropopause.

There is one important difference in the behavior expected in the ½O_3 and $2 \times CO_2$ experiments which remains, having nothing to do with "Drive," but with the response. Comparing Eqs. (B3) and (B8) we see that the ½O_3 involves τ for $1 \times CO_2$, while the $2 \times CO_2$ involves τ', i.e., the $2 \times CO_2$ transmission functions. In the mesosphere and upper stratosphere, $2 \times CO_2$ cooling rates are a factor of $\sim$1.3 greater than $1 \times CO_2$ rates, so that the 2× response *to a given* δJ will be smaller by a factor of $\sim$0.7 than the corresponding 1× response in that region. For this reason, as well as the fact that $\delta J_{sw} + \delta Q_{9.6}$ is larger than $(\delta J)_{\text{eff}}$, we expect that the ½O_3 thermal response at the stratopause should be nearly a factor of 2 larger than that due to doubling of CO_2.

APPENDIX C

A Simple Model of Radiative and Dynamical Adjustment

The response of a simple linear model to perturbations in the heating function provides an interesting illustration of dynamical and radiative adjustment. We consider a hydrostatic, zonally symmetric model atmosphere on an equatorial β-plane, and assume that the zonal wind is in geostrophic balance with the pressure field. As discussed in Section 5, this last approximation is well satisfied in the GCM. Newtonian cooling, with uniform time constant τ_r, damps thermal perturbations, while Rayleigh friction, with constant decay time τ_m, acts to bring $\bar{U}$ to zero. We may assume that there is an eddy forcing term $\bar{F}$ which drives $\bar{U}$, and a meridionally symmetric heating $\bar{J}$ which forces the thermal field $\bar{T}$. $\bar{J}$ may be considered the sum of eddy heating and that due to purely symmetric forcing. We work in log p coordinates, with $z = -H \times \log p$, H being a constant mean scale height and $w = Dz/Dt$.[14]

With these assumptions, the steady state equations are

$$-f\bar{v} = -\bar{U}/\tau_m + \bar{F}, \quad \text{(C1)}$$

$$f\bar{U} = -\frac{\partial\bar{\Phi}}{\partial y}, \quad \text{(C2)}$$

$$H\frac{\partial\bar{\Phi}}{\partial z} = +R\bar{T}, \quad \text{(C3)}$$

[13] B and τ are the control experiment quantities, while B' and τ' are the perturbed Planck function and transmission function; then $B'\tau' - B\tau = (B' - B)\tau' + B(\tau' - \tau) \equiv \delta B\tau' + B\delta\tau$ is an identity.

[14] This model is very similar to one used by Dickinson (1971) in an investigation of the dynamics of the Hadley circulation.

$$\frac{\partial \bar{v}}{\partial y} + \frac{\partial \bar{w}}{\partial z} - \frac{\bar{w}}{H} = 0, \tag{C4}$$

$$\bar{w}\left(\frac{g}{c_p} + \frac{\partial T_0}{\partial z}\right) = \bar{J} - \bar{T}/\tau_r. \tag{C5}$$

Here T_0 is the temperature of the basic state, assumed independent of y, and R is the reduced gas constant.

The continuity equation is satisfied by the introduction of a streamfunction ψ such that

$$\bar{v} = e^{z/2H}\left(\frac{\partial \psi}{\partial z} - \frac{1}{2H}\psi\right), \tag{C6a}$$

$$\bar{w} = -e^{z/2H}\frac{\partial \psi}{\partial y}. \tag{C6b}$$

By use of (C1–C4), the thermodynamic equation may be written as

$$\frac{\tau_r}{\tau_m} N^2 \frac{\partial \bar{w}}{\partial y} - f^2 \frac{\partial \bar{v}}{\partial z} = f\frac{\partial \bar{F}}{\partial z} + \frac{\tau_r}{\tau_m}\frac{R}{H}\frac{\partial \bar{J}}{\partial y}, \tag{C7}$$

where

$$N \equiv \left[\left(\frac{g}{c_p} + \frac{\partial T_0}{\partial z}\right)\frac{R}{H}\right]^{1/2},$$

and approximately equals the Brunt-Väisälä frequency.

We now imagine that $\bar{J}$ is perturbed, due, for example, to ozone reduction. We shall also assume that $\bar{F}$, the eddy momentum forcing, has not changed, as is approximately the case in our GCM simulation. Denoting the changes in $\bar{J}$, $\bar{v}$ and $\bar{w}$ by the prefix δ, the perturbation now satisfies

$$\frac{\tau_r}{\tau_m} N^2 \frac{\partial}{\partial y}\delta\bar{w} - f^2 \frac{\partial}{\partial z}\delta\bar{v} = \frac{\tau_r}{\tau_m}\frac{R}{H}\frac{\partial}{\partial y}\delta\bar{J}. \tag{C8}$$

The first term comes from $\delta\{[(g/c_p) + (\partial T_0/\partial z)]\bar{w}\}$ in Eq. (C5), and the second from $\delta(\bar{T}/\tau_r)$.

The appearance of the y derivative of $\delta\bar{J}$ in Eq. (C8) reflects the fact that only horizontal temperature *gradients* lead to meridional motions, and thus to changes in the dynamical heating. In this model, the response to a $\delta\bar{J}$ which is constant in y will simply be a purely radiative temperature change $\delta\bar{T} = \tau_r\delta\bar{J}$. What is at issue is not whether there will be such a radiative response, but rather, whether the system will respond to a non-constant $\delta\bar{J}$ radiatively or dynamically.

The character of this response is determined by the relative size of the two terms on the left-hand side of Eq. (C8). If the first term [involving $(\partial\delta\bar{w}/\partial y)$] dominates, the adjustment is dynamical, while if $f^2(\partial\delta\bar{v}/\partial z)$ dominates, then it is the temperature field which has changed, and the adjustment is radiative [see Eq. (4.2)].

A simple example involves a source perturbation of vertical scale D of the form

$$\delta\bar{J} = \delta\tilde{J}(y)e^{z/2H}\sin(z/D). \tag{C9}$$

Introduction of the streamfunction $\tilde{\psi}(y) = \psi(y,z)/\sin(z/D)$ then leads to

$$\frac{\partial^2}{\partial y^2}\delta\tilde{\psi} - y^2\frac{\tau_m}{\tau_r}\frac{\beta^2}{N^2H^2}\left(\frac{H^2}{D^2} + \frac{1}{4}\right)\delta\tilde{\psi} = \frac{R}{HN^2}\frac{\partial}{\partial y}\delta\tilde{J}. \tag{C10}$$

The critical horizontal scale in this equation is

$$L_c = \left(\frac{NH}{\beta}\right)^{1/2}\left[\left(\frac{\tau_m}{\tau_r}\right)\left(\frac{H^2}{D^2} + \frac{1}{4}\right)\right]^{-1/4},$$

since (C10) can be written as

$$\frac{\partial^2}{\partial\eta^2}\delta\tilde{\psi} - \eta^2\delta\tilde{\psi} = \frac{RL_c}{HN^2}\frac{\partial}{\partial\eta}\delta\tilde{J}, \tag{C11}$$

where $\eta = y/L_c$. For $\tau_m/\tau_r \sim 1$, and $D \geq H$, L_c is on the order of 2000 km.

It is reasonable to expect that for $\eta^2 \ll 1$, the $(\partial^2\delta\tilde{\psi}/\partial n^2)$ term in Eq. (C11) should dominate, while for $\eta^2 \gg 1$, the $\eta^2\delta\tilde{\psi}$ term is the important one. This may be verified by examining a simple case in which $(\partial\delta\tilde{J}/\partial\eta)$ is proportional to η. (Note that in an annual-average model, $\tilde{J}$ must be an even function of η.) The results of a numerical integration show that for $\eta = 0.5$, about 85% of the forcing is balanced by the derivative term; at $\eta = 1.0$, 53%; while at $\eta = 2.0$, only 6%.

The analysis therefore suggests that for $y \gg L_c$, the adjustment will be purely radiative, even in the case where $(\partial\delta\bar{J}/\partial y) \neq 0$. It is only for $y \leq L_c$ that there will be an appreciable dynamical response to altered heating. We thus expect the strongest dynamical response in the tropics, even though that is a region in which the *mean* temperature is under strong radiative control.

REFERENCES

Ackerman, M., 1971: Ultraviolet solar radiation related to mesospheric processes. *Mesospheric Models and Related Experiments*, D. Reidel, 149–159.

Blake, D., and R. S. Lindzen, 1973: Effect of photochemical models on calculated equilibria and cooling rates in the stratosphere. *Mon. Wea. Rev.*, **101**, 783–802.

Boughner, R. E., 1978: The effect of increased carbon dioxide concentrations on stratospheric ozone. *J. Geophys. Res.*, **83**, 1326–1332.

CIRA, 1965: *Cospar International Reference Atmosphere*. N. Holland Publ. Co., 313 pp.

Dickinson, R. E., 1969: Theory of planetary wave-zonal flow interaction. *J. Atmos. Sci.*, **26**, 73–81.

——, 1971: Analytic model for zonal winds in the tropics. I. Details of the model and simulation of gross features of the zonal mean troposphere. *Mon. Wea. Rev.*, **99**, 501–510.

——, 1974: Climate effects of stratospheric chemistry. *Can. J. Chem.*, **52**, 1616–1624.

Fels, S. B., 1979: Simple strategies for inclusion of Voigt effects in infrared cooling rate calculations. *Appl. Opt.*, **18,** 2634–2637.

——, and L. D. Kaplan, 1975: A test of the role of longwave radiative transfer in a general circulation model. *J. Atmos. Sci.*, **33,** 779–789.

——, and M. D. Schwarzkopf, 1975: The simplified exchange approximation: a new method for radiative transfer calculations. *J. Atmos. Sci.*, **32,** 1475–1488.

——, and ——, 1980: An efficient, accurate algorithm for calculating CO_2 15 μm cooling rates. Accepted for publication in *J. Geophys. Res.*

Groves, K. S., S. R. Mattingly and A. F. Tuck, 1978: Increased atmospheric carbon dioxide and stratospheric ozone. *Nature*, **273,** 711–715.

Haigh, J. D., and J. A. Pyle, 1979: A two-dimensional calculation including atmospheric carbon dioxide and stratospheric ozone. *Nature*, **279,** 222–224.

Hartmann, D. L., 1976: The dynamical climatology of the stratosphere in the Southern Hemisphere during late winter 1973. *J. Atmos. Sci.*, **33,** 1789–1802.

——, 1978: A note concerning the effect of varying extinction on radiative-photochemical relaxation. *J. Atmos. Sci.*, **35,** 1125–1130.

Holloway, J. L., and S. Manabe, 1971: Simulation of climate by a global general circulation model: I. Hydrologic cycle and heat balance. *Mon. Wea. Rev.*, **99,** 335–370.

——, M. J. Spelman and S. Manabe, 1973: Latitude-longitude grid suitable for numerical time integration of a global atmospheric model. *Mon. Wea. Rev.*, **101,** 69–78.

Kurihara, Y., and J. L. Holloway, 1967: Numerical integration of a nine-level global primitive equations model formulated by the box method. *Mon. Wea. Rev.*, **95,** 509–530.

Lacis, A. A., and J. E. Hansen, 1974: A parameterization for the absorption of solar radiation in the earth's atmosphere. *J. Atmos. Sci.*, **31,** 118–133.

Leovy, C., 1964: Radiative equilibrium of the mesosphere. *J. Atmos. Sci.*, **21,** 238–248.

Lindzen, R. S., and R. Goody, 1965: Radiative and photochemical processes in mesospheric dynamics: Part I. Models for radiative and photochemical processes. *J. Atmos. Sci.*, **22,** 341–348.

Luther, F. M., D. J. Wuebbles and J. S. Chang, 1977: Temperature feedback in a stratospheric model. *J. Geophys. Res.*, **82,** 4935–4942.

Mahlman, J. D., and W. J. Moxim, 1976: A method for calculating more accurate budget analyses of "sigma" coordinate model results. *Mon. Wea. Rev.*, **104,** 1102–1106.

——, H. Levy II and W. J. Moxim, 1980: Three-dimensional tracer structure and behavior as simulated in two ozone precursor experiments. *J. Atmos. Sci.*, **37,** 655–685.

Manabe, S., and B. G. Hunt, 1968: Experiments with a stratospheric general circulation model. I. Radiative and dynamic aspects. *Mon. Wea. Rev.*, **96,** 477–502.

——, and J. D. Mahlman, 1976: Simulation of seasonal and interhemispheric variations in the stratospheric circulation. *J. Atmos. Sci.*, **33,** 2185–2217.

——, and R. T. Wetherald, 1967: Thermal equilibrium of the atmosphere with a given distribution of relative humidity. *J. Atmos. Sci.*, **24,** 241–259.

Newell, R. E., J. W. Kidson, D. G. Vincent and G. J. Boer, 1972: *The General Circulation of the Tropical Atmosphere and Interactions with Extratropical Latitudes*, Vol. 1. The MIT Press, 258 pp.

Ramanathan, V., 1976: Radiative transfer within the earth's troposphere and stratosphere: A simplified radiative-convective model. *J. Atmos. Sci.*, **33,** 1330–1346.

——, and R. E. Dickinson, 1979: The role of stratospheric ozone in the zonal and seasonal radiative energy balance of the earth-troposphere system. *J. Atmos. Sci.*, **36,** 1084–1104.

——, L. B. Callis and R. E. Boughner, 1976: Sensitivity of surface temperature and atmospheric temperature to perturbations in the stratospheric concentration of ozone and nitrogen dioxide. *J. Atmos. Sci.*, **33,** 1092–1112.

Reck, R. A., 1976: Stratospheric ozone effects on temperature. *Science*, **192,** 557–559.

Sangster, W. E., 1960: A method of representing the horizontal pressure force without reduction of station pressures to sea level. *J. Meteor.*, **17,** 166–176.

Schoeberl, M. R., and M. A. Geller, 1977: A calculation of the structure of stationary planetary waves in winter. *J. Atmos. Sci.*, **34,** 1235–1255.

——, and D. F. Strobel, 1978: The response of the zonally averaged circulation to stratospheric ozone reductions. *J. Atmos. Sci.*, **35,** 1751–1757.

Strobel, D. F., 1977: Photochemical-radiative damping and instability in the stratosphere. *Geophys. Res. Lett.*, **4,** 424–426.